OLUMIDE ONI T. Ph.D. Analysis of Periodic Oscillations of APDs in Reaction Diffusion Waves with Nonlinear Diffusion in Tissues with Peripheral Nerve Injury (PNI). (2023) Directed by Dr. Joseph Starobin. 80 pp.

Millions of people suffer from peripheral nerve injury every year. Previous works have predominantly focused on surgical means of injury treatment without sufficient attention to studying distinct mechanisms of electrical conduction in small peripheral nerves. In this study, we examined the effects of nonlinear diffusion on wave propagation generated in normal and injured (with altered electrical conduction) peripheral nerves using one-dimensional Fitzhugh-Nagumo model. We modified this model by adding an additional power function type nonlinear diffusion term to account for fundamental changes in charge balance in excitable cells of small peripheral nerves. It was found that nonlinear diffusion played a critical role in stabilization of action potential propagation in healthy and injured peripheral nerves. In addition, it was observed that conditions for stable propagation of action potential in injured nerves significantly depended not only on the magnitude of nonlinear diffusion but also on location of zones of injury. These results may be helpful in elucidating physiological mechanisms of various electrical conduction pathologies which occur in injured peripheral nerves.

ANALYSIS OF PERIODIC OSCILLATIONS OF APDS IN REACTION

DIFFUSION WAVES WITH NONLINEAR DIFFUSION IN TISSUES WITH

PERIPHERAL NERVE INJURY (PNI)

by

Olumide Oni T.

A Dissertation
Submitted to
the Faculty of The Graduate School at
The University of North Carolina at Greensboro
in Partial Fulfillment
of the Requirements for the Degree
Doctor of Philosophy

Greensboro

2023

Approved by

Dr. Joseph Starobin
Committee Chair

DEDICATION

To Esther, Samuel, and Samantha - my moon, my star, my everything.

APPROVAL PAGE

This dissertation written by Olumide Oni T. has been approved by the following committee of the Faculty of The Graduate School at The University of North Carolina at Greensboro.

Committee Chair

_____
Dr. Joseph Starobin

Committee Members

_____
Dr. Hemali Rathnayake

_____
Dr. Tetyana Ignatova

_____
Dr. Eric Josephs

March 21, 2023
_____
Date of Acceptance by Committee

February 24, 2023
_____
Date of Final Oral Examination

iv

ACKNOWLEDGEMENTS

TABLE OF CONTENTS

LIST OF TABLES

LIST OF FIGURES

CHAPTER I: INTRODUCTION

About twenty million Americans suffer from peripheral nerve injury caused by trauma and medical disorders. The cost effect of nerve injury is vast. Statistics show that nerve injuries result in roughly $150 billion in annual healthcare dollars in the United States. Beyond the cost in dollars, severe nerve injury can have very devastating effects on the quality of life of patients. In most cases, surgical repair procedures with gene therapy are peripheral nerve injuries usually require surgical nerve reconstruction. Unfortunately, motor, and sensory functions recovery after a peripheral nerve injury are subpar, even after a surgical procedure to repair the damage. A meta-analysis of median and ulnar nerve repairs in 2005 demonstrated that only 52.6% achieved satisfactory motor recovery, with even less 42.6% experiencing satisfactory sensory recovery[1]. The poor repair is due to the slow rate of axonal elongation during regeneration and atrophic changes in denervated Schwann cells and target muscles with proximal lesions[2]. Thus, even a surgical procedure is barely adequate for proper healing after a severe peripheral nerve injury.

In this body of work, we will study the effects of nonlinear diffusion on wave propagation generated in normal and injured tissues using a one-dimensional Fitzhugh-Nagumo model. Changes in Action Potential Durations (APDs) and Repolarization Intervals (RIs) will be observed based on this modification. Notably, adding a quadratic or quartic transmembrane potential-dependent diffusion component will affect the Fitzhugh-Nagumo model's diffusion term. It will no longer be a constant diffusion. While many models help study nonlinear dynamics in biological systems, we chose to use the Fitzhugh-Nagumo model with the nonlinear diffusion term for two primary reasons. One is its simplicity. It is well known that the Fitzhugh-Nagumo model is a two-dimensional simplification of the 4-variable Hodgkin-Huxley model.

Secondly, modifying the Fitzhugh-Nagumo model to include a nonlinear diffusion term means we can account for relative charge depletion that usually occurs in small peripheral nerves, typically with a diameter less than 1.5mm. While the Hodgkin-Huxley model is the gold standard in qualitatively explaining the action potential dynamics in nerve cells, it is, unfortunately, unable to account for this charge depletion in peripheral nerves.

Next, we will introduce an inhomogeneous injury profile into our 1D nerve fiber and study the action potential propagation within this region. Finally, we will stabilize the propagation by introducing an external stimulation as a periodic function and adding current at the left end of the cable. We will then observe the oscillations of APD and RI through this injury region, the nonlinear oscillations of the Basic Cycle Length's end (BCL_{end}) and its dependances on the linear component of the diffusion term for the nonlinear quadratic diffusion at different amplitudes of injury in PNs.

While several works have studied the propagation of action potential in axonal neurons, none has focused on analysis of action potential propagation within peripheral nerves with or without injuries. This work aims to bridge this significant gap.

Important Terms and Definitions
Dynamical, Linear and Nonlinear systems

The works discussed in this thesis are focused on nonlinear dynamical systems modeling. Modeling these kinds of systems is helpful because it enables us to predict how multiple components of a system will interact over time as viewed within a single system. To understand the term *dynamical systems*, it will be helpful to break it down into its component words.

The "*dynamic*" part indicates that this will evolve with **time**. That is, time is an essential component of the model/system being considered. Models that describe dynamic systems assume that the system's current state depends on the past[3]. The conventional static systems tend to ignore the time component of the system. As a result, the studied variables cannot be fully understood as their evolution through time cannot be well considered. However, we can fully explore this evolution in dynamical systems in time. A deeper look will quickly show that the time component is fundamental to a robust understanding of the system and the basic structure of the system's data. While time series models can represent how a system evolves in some other models, time-series data is not necessary for testing such models. Even at that, the importance of time in such models should not be ignored as it plays a critical role. This is because response time distributions are considered in model formulation and predictions (e.g., simultaneous modeling of choice probability and choice response time when predicting choice behavior)[3].

The "*system*" part of dynamic systems signifies that we have many moving parts. This only shows us that we are dealing with an environment where many components interact as a part of a larger ensemble. While tending to behave complexly, these systems have defined rules that tend to guide their interaction and behavior such that it is in an orderly manner. Due to the complex nature of these systems, describing them becomes very difficult. One factor that researchers always consider in studying dynamical systems is their stability, as its determination is a fundamental concern that arises in almost all real situations that can be modeled or described by a dynamical system[4]. In understanding this, researchers try to understand how the system maintains its stability over time and to what extent or degree the system is stable.

Dynamical systems can either be linear or nonlinear. We need to demarcate between linearity and nonlinearity in dynamical systems. Perhaps it is helpful to understand

mathematically what it means for a function or system to be linear or nonlinear. The concept of both is found throughout the field of research. To understand this, let us simplify by defining a linear function in one dimension. Let us consider a function f that is said to be linear. The function f is such that:

$$f: \mathbb{R} \rightarrow \mathbb{R} \tag{1a}$$

$$f = f(x) \; \forall \, x \in \mathbb{R} \tag{1b}$$

If f is genuinely linear, then it will fulfill the following conditions:

$$f(\alpha x) = \alpha f(x) \; \forall \, x \in \mathbb{R}, \qquad \alpha \in \mathbb{R} \tag{2a}$$

$$f(a + b) = f(a) + f(b) \; \forall \, a, b \in \mathbb{R} \tag{2b}$$

If any of the conditions above is not fulfilled, then f is nonlinear. Thus, we can define a *linear system* as a system where the set of variables describing the past state can be combined linearly to describe the current state. On the other hand, a *nonlinear system* does not have the current state expressed fully as a linear combination of variables of the past or previous state. In nonlinear systems, it is quite possible to express some of the variables of the current state as a linear combination of the variables of the previous state. However, to capture all variables' dependencies, we would need extra descriptive steps and techniques to achieve this. Therefore, the focus of this thesis is a nonlinear dynamical system. We focus on this dynamical system as it applies to neuron excitation to narrow it down even further.

Excitability

Excitability is a term used to describe the ease with which a cell responds to a stimulus with a regenerative action potential[5]. Excitability is found almost everywhere in the body and is essential to maintaining life. In the general sense of the word, all specialized cells of a complex organism like the human body have some form of excitability as they all perform a specific action on receipt of external signals. Specifically, however, some cells in the human body are significantly responsive to an external signal and primarily use this feature of excitability to perform their primary functions in the body. Therefore, these cells are of high significance when studying the concept of excitability. Cells such as neurons, the brain cells, cardiac cells, and pancreatic b-cells use this excitability property to function correctly and maintain health. In these cells, electrical activity manifests in electroencephalograms and electrocardiograms, but the sources of this activity are at the cellular level[6]. Excitability results from the distribution (concentration) and motion of charged ions across the permeable membrane in the cell. During this process of excitation of cells, there is the resting state, the excited state, the refractory state, and the recovery state.

Excitability is a phenomenon that can also be observed in nature. An example of excitability existing in nature is forest fires[7]. Consider a forest of trees. Each tree in the forest can possibly be in any of the states: resting, excited, refractory, and recovery states. A tree in its resting state is healthy and unburnt. A fire happens, and then the tree goes into an excited state. In this state, wave propagation is possible in two dimensions where the excited tree will transmit its excitation to its nearest neighbors. Thus, the fire propagates through the process of diffusion. This excited state is followed by a refractory state where the tree is no longer responsive to fire. Through regrowth, the forest returns to its original state after a while, which is the recovery state. Another simple example of excitability in nature is the household match. The chemical

components in the match head are stable to small fluctuations in temperature. However, a

fluctuation large enough, for example, friction between the head and a rough surface, can ignite

or excite the head, thus releasing heat and light[8,9]. The match goes through almost all the states

except recovery.

The anatomy of the Neuron

Neurons or nerve cells are the foundation of communication in the body. They are the

building blocks of the nervous system. The human brain alone contains approximately 100

billion neurons[10]. Neurons are highly specialized cells responsible for receiving sensory input

from outside the body, sending motor commands to our muscles, and transforming and relaying

the electrical signals at every step in between[11]. All neurons have three major parts:

1. The dendrites

2. The cell body (also called soma)

3. The axons

Asides from these three major parts, there is also the axon terminal and the synapse at the

end of the Neuron. Figure 1 shows the parts of a neuron.
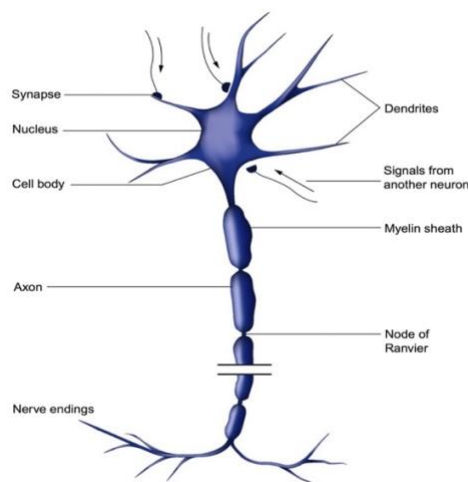
Figure 1 - Parts of a neuron. Reproduced from[12]

The *dendrites* connect to other neurons and receive signals from them. The cell body organizes and keeps the cell functional, while the axon, a fiber, is responsible for transferring signals to other cells and organs.

Neurons are usually classified based on their functions. There are three types of nerves in the body:

1. Autonomic nerves: These nerves control involuntary or partially involuntary activities in the body. These activities include heart rate, digestion, temperature control, heart rate.

2. Motor nerves: These nerves carry messages between the brain and muscles to make the body move.

3. Sensory nerves: Sensory nerves carry messages between the brain and different body parts to signal sensations like pain, temperature, and pressure.

The Anatomy of the Peripheral Nerve

Peripheral nerves transmit signals between the spinal cord and the other parts of the body. The peripheral nervous system comprises of three types of cells: the neuronal cells, the glial cells and the stromal cells[13].

In the adult state, the physical structure of a peripheral nerve can be best divided into five segments:

1. The cell body and axon

2. Schwann cell

3. Connective tissue sheath

4. Vascularity

5. End organs, sensory and motor

In the maintenance and functions of peripheral nerves, there are key roles played by other cells other than neurons. For example, the Schwann cells that sheaths the nerves also provides trophic support through the release of important neurotrophs like Nerve Growth Factor (NGF)[13].

The axons and Schwann cells are grouped into fascicles, sheathed by the perineurium[14]. A sheath of tissue protects the nerve just like insulation around an electrical cable. This is called the *myelin sheath*. The role of the *myelin sheath* is to improve conduction velocity. It does this by limiting the sites of ionic transfer along the axon of the nodes of Ranvier, thereby resulting a faster action potential propagation. This is referred to as "saltatory conduction"[13]. Axons are separated into bundles inside the nerve. Tissue layers separate each bundle. The fiber breaks when an injury occurs due to pressure or stretching. When this cut in the nerve occurs (nerve injury), the nerve and the insulation are severed.
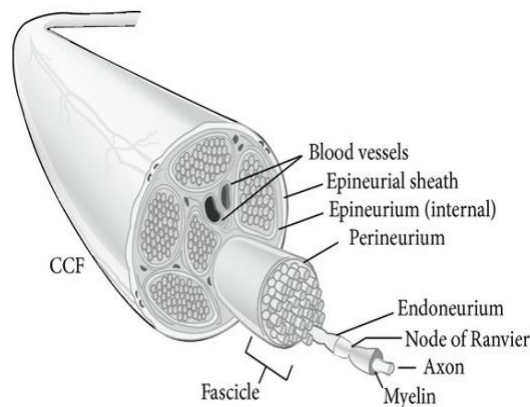
Figure 2 - Anatomy of a peripheral nerve[1]

In some cases, the fibers inside the nerve might break while the protective sheath remains intact. If the insulating sheath stays intact, then the end of the fiber distal from the brain dies while the one proximal to the brain survives. In this case, a regeneration might occur. After some time, the nerve may begin to heal with new fibers growing beneath the insulation until it reaches

a muscle or sensory receptor. The figure 3 below shows degeneration and regeneration after a peripheral nerve injury.
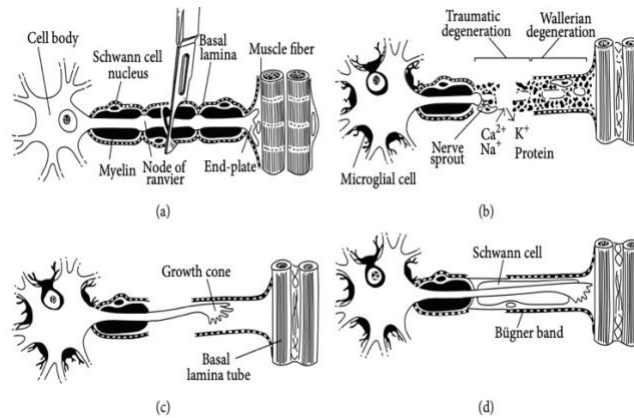
Figure 3 - Damaged PN undergoing regenerative processes[15]

Action Potential (AP) and Polarization

Neurons, as excitable cells in the human body, can undergo transient polarization and depolarization. They behave so that a brief electrical pulse can make the transmembrane potential experience an elevation. This elevation, when prolonged, is called the **action potential**. An action potential is a sudden and transient depolarization of the membrane[16]. Only neurons and muscle cells like those of the heart are capable of generating an action potential. In neurons, the action potentials are generated to transmit nerve signals to targeted muscles, tissues, and other neurons. Action potentials just do not happen. There are steps involved in the generation and propagation of action potential. The first thing to note is that not all electrical excitations or stimuli can create an action potential. There can be a *subthreshold*, a *threshold*, and a *suprathreshold* stimulus. Action potential follows the all-or-nothing law meaning that when the membrane potential is not up to the threshold potential, no action potential is produced. The

threshold and suprathreshold stimuli have high enough energies to result in the production of an action potential. The threshold potential usually ranges from -50 to -55 mV. Membrane potential typically varies depending on cell type. For the Neuron, it usually sits between -50 to -75 mV. This value is usually determined by the relative ratio of ions (in the case of the Neuron $Na+$ and $K+$, extracellular to intracellular, permeability of the membrane to ions, and various negatively charged intracellular proteins and organic phosphates that cannot cross the cell membrane)[17,18]. Both sodium's and potassium's voltage-gated channels are closed in the resting state. Voltage-gated channels will only open and close depending on the difference in voltage across the cell membrane. Hence the term "voltage-gated". While in the resting state, membrane potential increases due to its permeability to K+. Voltage-gated sodium ion channels open because of the electrical stimulus. This causes the Na+ ions to rush into the cell. As a result, the inside of the cell becomes more electropositive compared to the outside of the cell. An action potential is propagated if this continues such that the threshold potential is reached.

An action potential has a few phases, hyperpolarization, depolarization, overshoot, repolarization, and hyperpolarization. *Ab-initio*, the cell at resting potential is in the **resting** phase, as seen in figure 2 below. In this phase, the initial increase in the membrane potential to the threshold potential occurs. As described previously, the voltage-gated sodium ion channels open up due to the increased membrane potential in the previous hyperpolarization phase, and Na+ ions rush into the cell. This causes a short-term positive feedback loop where the increasing voltage causes more voltage-gated Na+ ion channels to open. This phase is called the **depolarization** phase, and it is here that the cell gets more electropositive. This electropositive event continues till the potential gets closer to the electrochemical equilibrium of Na, which is approximately about +61mV. At this point, the cell is no longer responsive to potential, and this

phase of intensive positivity is called the overshoot phase. Sodium channels close very quickly. This quick closure results in the sudden decrease of permeability of the cell membrane to Na+ ions. Potassium's voltage-gated channels open, which in turn causes K+ ions to rush in. this significant potassium efflux causes a decrease in the cell's electropositivity. This phase is called the **repolarization** phase. During this phase, the cell attempts to attain its potential by resting again. However, potassium's voltage-gated channels close a lot slower than sodium's. As a result, the decrease in electropositivity of the cell continues till it enters the **hyperpolarized** phase again. Here, the membrane potential attained is more negative than the membrane potential before the action potential is generated. Slowly due to leak channels, the cell attains its resting potential.
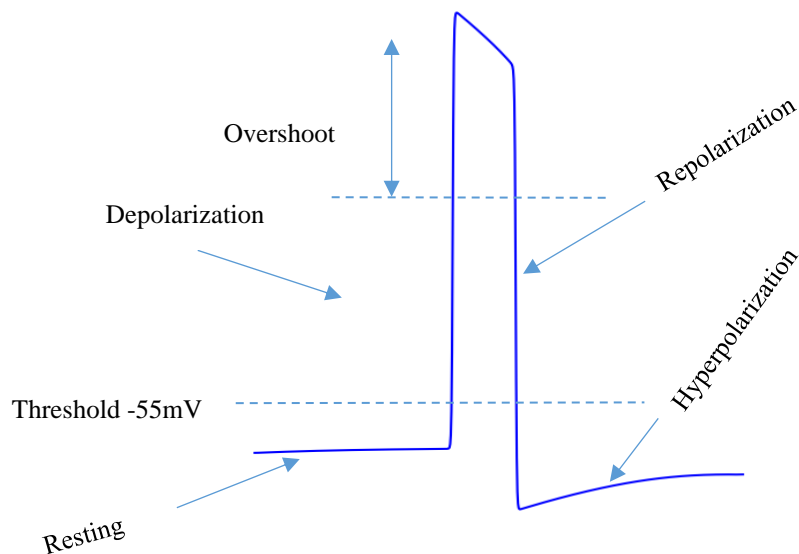
Figure 4 - Action potential curve and phases

After an action potential is generated, there is a period during which the Neuron is unresponsive to potential and thus cannot generate another action potential. This period is called **the refractory period**.

Action Potential Duration (APD) and Repolarization Interval (RI)

The Repolarization Interval (RI) is the interval between successive action potentials, while Action Potential Duration (APD), as the name suggests, is the time duration of a single action potential. The Basic Cycle Length (BCL) is simply a summation of RI and APD. The physical relationship between these three is shown in the figure 5 below.
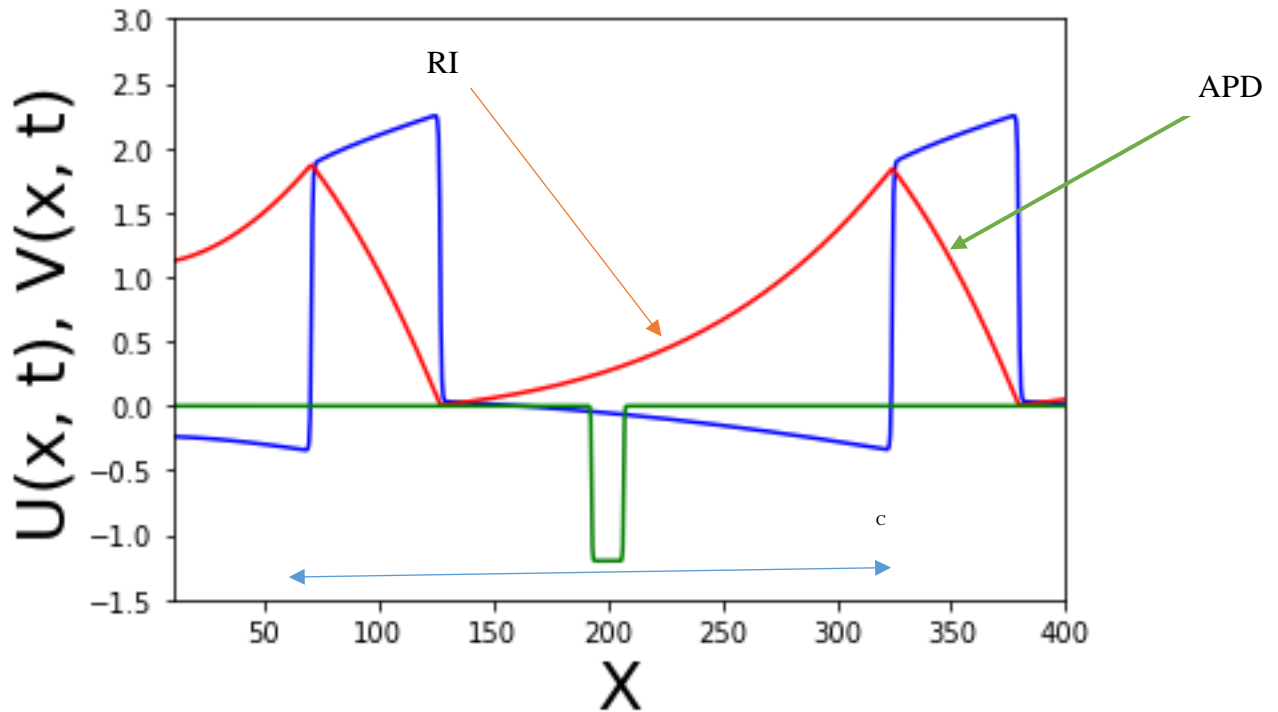
Figure 5 - Two successive action potentials in a nerve cable with injury at the center, showing the relationship between RI, APD and BCL is the sum of RI and APD.

In excitable media, if a second excitation is initiated too soon after the previous one, the duration of the second pulse is considerably shorter than the first[19]. In biological excitable media, an APD restitution curve describes the relationship between the APD and the interval between two excitations that follow each other[20]. In restitution, Action Potentials (APs) initiated at relatively short RIs will lead to shorter APDs.
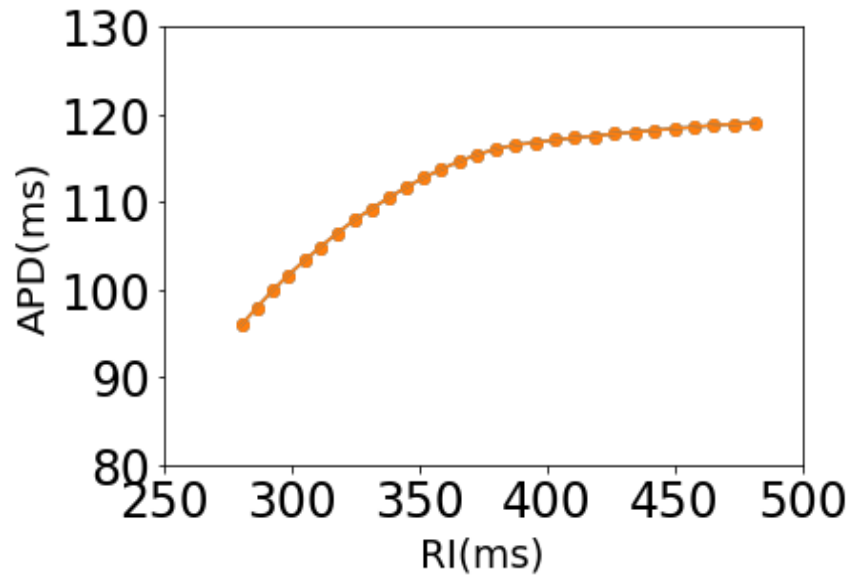
Figure 6 - An example of a restitution curve showing the relationship between APD and RI

Major Reaction-Diffusion Models to Describe Excitability of Cellular Membranes

Different models can be used to understand the overwhelming structural complexity of the neuronal processes and gain a better understanding of their dynamics. The Nobel prize-winning Hodgkin Huxley model (HH) is beneficial for this purpose. Since the groundbreaking discoveries of Hodgkin and Huxley in 1952, there has been an enormous amount of interest in and motivation for studying and understanding dynamical systems. This motivation has produced some exciting models. Some of the most successful of them in the area of biophysics are

Hindmarsh-Rose (HR), Fitzhugh-Nagumo (FN), and Morris-Lecar (ML). HR and FN are particularly very successful in capturing neural firing behavior.

Reaction-Diffusion Systems

Reaction-diffusion (RD) systems occur in many areas of sciences and engineering. We see reaction-diffusion systems in biological, chemical, physical, etc. There are different methodologies from several areas of mathematics and physics with valuable tools for studying these systems. To mention just a few, some of these methods are numerical analysis, singular perturbation, bifurcation, and stability theory. To derive a reaction-diffusion system, we can start with *Fickian diffusion*. This says that the flux of a material which can be the amount of chemicals, cells, number of animals, etc., denoted by J, is proportional to the gradient of the concentration of the material[34]. In one dimension:

$$J \propto \frac{\partial c}{\partial x} \quad \Rightarrow J = -D \frac{\partial c}{\partial x} \tag{3a}$$

In general,

$$\boldsymbol{J} = -D \nabla c \tag{3b}$$

where $c = c(x, t)$ is the concentration of the species and D is its diffusivity. The negative in the equation signifies that the diffusion transports material from a high to low concentration region. Now, if we consider diffusion in three dimensions, and we let S be an arbitrary space enclosing a volume V, then applying the general conservation law, which dictates that the rate of

change of material in the volume V is equal to flow of materials across S into V with the material created in V added. Mathematically, this can be stated thus:

$$\frac{\partial}{\partial t}\int_V c(x,t)dv = -\int_S J.ds + \int_v fdv \tag{4}$$

Where f, the source of material, can be a function of c, x and t[34]. If we apply the divergence theory to the surface integral term on the right-hand side of the equation 4 above, and assuming that $c(x,t)$ is continuous, then equation 4 becomes:

$$\int_V \left[\frac{\partial c}{\partial t} + \nabla \cdot J - f(c,x,t)\right]dv \tag{5}$$

Considering that the integrand must be 0 since the volume is arbitrary, and using the generalized version of equation 3a (i.e., equation 3b), equation 5 therefore becomes:

$$\frac{\partial c}{\partial t} = f(c,x,t) + \nabla \cdot (D\nabla c) \tag{6}$$

where D could be a function of x and c. In a simple one-dimensional scalar case, the equation 5 above becomes:

$$\frac{\partial u}{\partial t} = f(u) + D\frac{\partial^2 u}{\partial x^2} \tag{7}$$

Where u is the concentration of materials, D is the diffusion coefficient which is usually taken as a constant, and $f(u)$ represents the local reaction kinetics. $f(u)$ can have different shapes and below we introduce a few of them:

- $f(u) = ku(1-u)$: Here k and D are positive parameters. This was suggested in 1937 by Ronald Fisher as a deterministic version of a stochastic model for the spatial spread of favored genes in a population[34,35]. Replacing $f(u)$ in equation 7 with this yields the *Fisher-Kolmogorov* equation.

15

- $f(u) = u(1 - u^2)$: This is well known as the Newell-Whitehead-Segel equation[36,37]. This equation describes the evolution of vertical velocity during perturbation from a stationary state. The vertical velocity is a slowing varying function of position and time.

The Hodgkin-Huxley Model

In 1952, Hodgkin and Huxley published five seminal papers that have since been the background reference in the studies of nonlinear dynamics in biological systems. These papers went ahead to describe a wide range of behaviors in the nerve of a giant squid. The first paper dealt with the experimental method of measurement, understanding of the current-voltage relationship, and behavior of the membrane of the Neuron in a normal ionic environment[21]. The second paper in the series discussed the ionic currents and described their resolution into currents of sodium and potassium. It also described the effects of changes in sodium concentration in the membrane. In a nutshell, it characterized the currents carried by the potassium and sodium ions[22]. The third paper describes the effect of sudden changes in potential on the time course of ionic conductance[21,23], i.e., what happens with each component of the membrane current when the time and duration of polarization/repolarization are varied. The fourth paper describes the inactivation process. This process reduces sodium's permeability gradually after it has undergone an initial rise as a result of depolarization and the action potential is now in its "falling phase"[24]. The series culminated in a final paper which harmonized all that had been discussed in the previous papers by showing quantitatively that the form and velocity of the action potential can be calculated from results from the previous four papers[21,25]. It effectively describes how membrane current applies critically to excitation and conduction in the squid's nerve.

16

In general, in order to describe this excitation, it is not sufficient to consider f(u) as quadratic and cubic functions. Hodgkin and Huxley constructed a specific electrical circuit which included 3 independent ionic currents as shown in the figure 7 below:
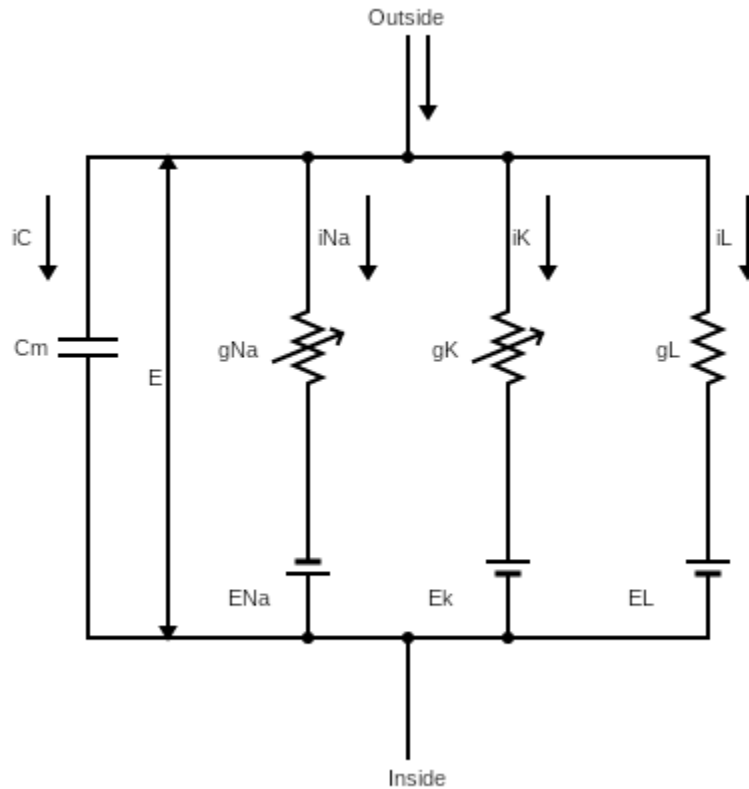
Figure 7 - An electrical circuit representation of the membrane with active sodium, potassium and leakage channels. Image was adapted from[25]

The cell membrane in this configuration, acts like a capacitor with constant capacitance of C_m. While conducting their experiments, Hodgkin and Huxley came to the determination that sodium and potassium ions (Na^+ and K^+) are the most critical components of the cell membrane as it concerns the generation of the action potential. As shown in the diagram above, both Na^+ and K^+ channels were determined to act as resistors. According to Hodgkin and Huxley, these resistances were described by voltage-dependent conductances (g_{Na} and g_k) thus:

17

$$R_{Na} = {}^1/_{g_{Na}}, R_K = {}^1/_{g_K} \tag{8}$$

Because of these resistances, the currents were also denoted as i_{Na} and i_k. A third ionic current called the leak current is designated as i_L. This current is a summation of other ionic currents present in the membrane, and a third conductance causes it called the leak conductance $(R_L = {}^1/_{g_L})$, which is independent of the membrane potential. E is the voltage across the capacitor, while separate electrical source batteries represent the Nernst potential for each ion with V_{Na}, V_k, and V_L. Suppose we apply Kirchhoff's law to the circuit diagram in figure 7. In that case, the conservation of charges will dictate that the external applied current I_{ext}, can be split into a sum of the ionic currents and the capacitive current i_c.

$$I_{ext} = i_{Na} + i_K + i_L + i_c \tag{9}$$

Where we can rewrite the capacitive current mathematically in terms of membrane capacitance and membrane potential V thus:

$$i_c = C_m \frac{dV}{dt} \tag{10}$$

The HH model is thus summarized in a system of four coupled ordinary differential equations where one is the equation for the membrane potential and three others for the channel gating variables:

$$C_m \frac{dV}{dt} = -\bar{g}_L(V - V_{leak}) - \bar{g}_{Na}m^3h(V - V_{Na}) - \bar{g}_k n^4(V - V_k) \tag{11a}$$

$$\frac{dn}{dt} = \emptyset[\alpha_n(v)(1 - n) - \beta_n(V)n] \tag{11b}$$

$$\frac{dm}{dt} = \emptyset[\alpha_m(v)(1 - m) - \beta_m(V)m] \tag{11c}$$

18

$$\frac{dh}{dt} = \emptyset[\alpha_h(v)(1-h) - \beta_h(V)h] \tag{11d}$$

Where $\bar{g}_k$ and $\bar{g}_{Na}$ are maximum conductances and *n, m* and *h* are gating variables with

values between 0 and 1. In the equations 11 above, we added a parameter ϕ, the *temperature*

factor. It is imperative to note here that the temperature at which the experiment is conducted is

critical. Because channels are stochastic in nature, they are sensitive to changes in temperature.

As a result, the rates of switching states depend exponentially on temperature. This is because

higher temperatures cause faster switching, and conversely, lower temperatures cause slower

switching[26]. In the equation 12 below, we mathematically define what ϕ is:

$$\emptyset = Q_{10}^{\frac{T-T_{base}}{10}} \tag{12}$$

Where Q_{10} is the ratio of the rates for an increase in temperature of 10°C. in the giant

squid's axon, $Q_{10} = 3$ and $T_{base} = 6.3°C$[26].

After their experimentation, Hodgkin and Huxley fit their experimental data and arrived

at the following expressions for the voltage-dependent rate constants:

$$\alpha_n(v) = \frac{0.01(v + 55)}{1 - e^{\frac{-(v+55)}{10}}}, \qquad \beta_n(V) = 1.125e^{\frac{-(V+65)}{80}} \tag{13a}$$

$$\alpha_m(v) = \frac{0.1(v + 40)}{1 - e^{\frac{-(v+40)}{10}}}, \qquad \beta_m(V) = 4e^{\frac{-(V+65)}{18}} \tag{13b}$$

$$\alpha_h(v) = 0.07e^{\frac{-(v+65)}{20}}, \qquad \beta_h(V) = \frac{1}{1 + e^{\frac{-V+35}{10}}} \tag{13c}$$

The table below shows the values of the constants parameters as derived experimentally:

Parameters	Values	Units
Membrane Capacitance (C)	1	$\mu F/cm^2$
Maximum Sodium Conductance $(\overline{g}_{Na})$	120	mS/cm^2
Maximum Potassium Conductance $(\overline{g}_K)$	36	mS/cm^2
Leak Conductance $(\overline{g}_L)$	0.3	mS/cm^2
Sodium Equilibrium Potential (V_{Na})	-115	mV
Potassium Equilibrium Potential (V_{Na})	12	mV
Leak Equilibrium Potential (V_L)	- 10.613	mV

Table 1: HH model constant parameters

The HH model has the advantage of being realistic and biophysically sound. It is excellent for describing and predicting many neuronal properties and behaviors. However, the HH in its original form is limited to the two voltage-dependent currents found in the squid giant axon, with only projections of its four-dimensional phase trajectories observable. Thus, it must be extended significantly to deal with neurons' excitable soma and dendrites. Also, the model

does not correctly capture the kinetics of the sodium ion channel, and it cannot account for the stochastic response to current injection resulting from the discrete nature of the ion channels[27]. As a result, more straightforward and better models are required to describe some neuronal properties and behaviors more adequately and holistically.

The Fitzhugh Nagumo Model

Since the publication of the seminal works and development of the Hodgkin-Huxley (HH) model in 1952, many other essential but simplified modifications to the HH model have emerged. Due to the complexity associated with the 4-variable system of the HH model, researchers worked to obtain simplifications that will still capture the critical dynamics of the action potential. The FitzHugh-Nagumo (FN) model is a two-dimension simplification of the Hodgkin-Huxley (HH) model proposed by R. FitzHugh and J. Nagumo in 1961. In 1961, the two-dimensional simplification presented by R. FitzHugh was obtained by his observation that the gating parameter *m* in the Hodgkin-Huxley model was significantly faster than the *n* and *h* variables. He also observed that the parameter *n + h,* as given by Hodgkin and Huxley, stays approximately constant during the propagation of action potential in the system. As a result of these observations, he was able to arrive at the following two-variable model, which he originally called the **Bonhoeffer-van der Pol (BVP)** model[28,29]:

$$\dot{x} = c(y + x - x^3/3 + z) \tag{14a}$$

$$\dot{y} = -(x - a + by)/c \tag{14b}$$

where

$$1 - 2b/3 < a < 1, \qquad 0 < b < 1, \qquad b < c^2$$

21

In a separate work by Nagumo *et al*[30] a prototype of a single cell excitable system was described in a similar way as equations 14. As a result, these two equations have since been referred to as the Fitzhugh-Nagumo model:

$$\frac{du}{dt} = f(u, v) \tag{15a}$$

$$\frac{dv}{dt} = \varepsilon g(u, v) \tag{15b}$$

There are many forms in which the FN model is represented. However, in our work, we choose to utilize it as:

$$\frac{\partial u}{\partial t} = f(u) + I + D\frac{\partial^2 u}{\partial x^2} \tag{16a}$$

$$\frac{dv}{dt} = \varepsilon(bu - \gamma v) \tag{16b}$$

Where *f(u)* is a third order polynomial that provides positive feedback, v is the slower recovery variables, γ and *b* are constant scaling parameters, u is the membrane potential, and *I* is the external stimulus current. The figure 8 below shows the phase plane for the FN model in equation 11 where $f(u) = u(a - u)(u - 1)$:
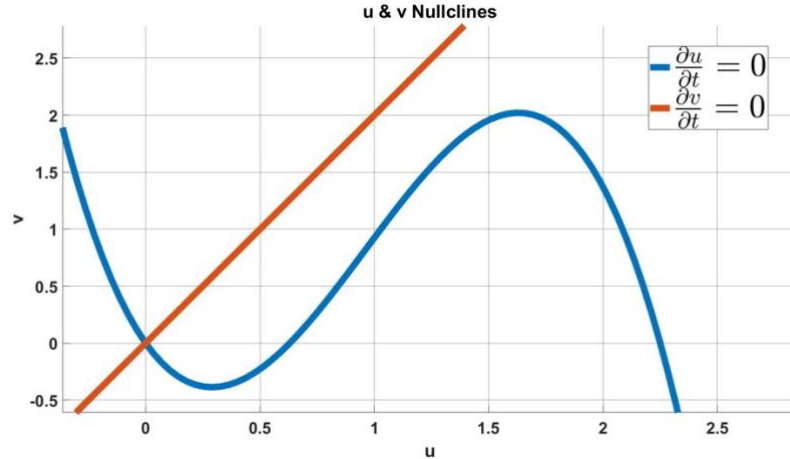
Figure 8 - A typical FN model phase portrait with a single equilibrium showing the u and v nullclines.

Figure 9 below illustrates 3 cases. The first (figure a) shows the phase plane when I is set to 0 in equation 12a. The second shows equation 3 without the diffusion present, i.e., $D = 0$ and with I again set to 0. This means that in the last figure of the 3 in figure 9,

$$f(u) = u(a - u)(u - 1) \tag{17}$$

Where the parameter a hold the values $0 < a < \frac{1}{2}$. The kinetic system may be classified as bistable, excitable, or oscillatory by the mechanism of nullclines intersections. The equation 16a and 16b above also gives the general Zeldovich-Frank-Kamenetzky (ZFK) equation[31] resulting from the combustion theory.

The FN model's simplicity allows the entire solution to be viewed at once. This is advantageous as it allows us to explain some fundamental biological phenomena related to neuronal excitability.
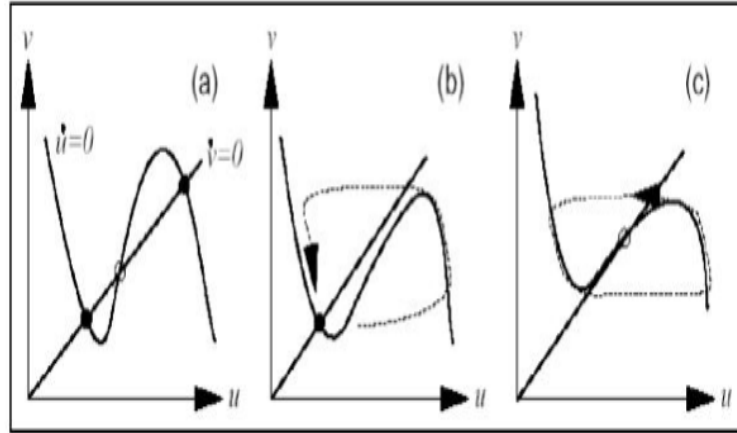
Figure 9 - Showing the phase portrait for equation 1 with I set to 0. This image was produced from[32]

Numerical Methods Review

In many differential equation problems as FN model, getting an analytical result is not always possible. In some cases, there are limitations due to the complexity of geometries. Therefore, numerical methods are essential tools to obtain solutions explicitly to such problems. Numerical methods analysis allows us to closely model experimental and practical situations[33]. Even when analytical solutions are possible, they might be challenging to solve. Numerical methods also help us to verify and validate the accuracy of results obtained from analytical solutions to problems. In this section, we briefly explain the finite difference methods for the simulation of differential equation such as FN model.

The Finite Difference Method

The Finite Difference Method (FDM) is one of the most straightforward numerical techniques for solving differential equations. The main idea here is to approximate derivatives with their finite-difference. FDM is a valuable tool for solving differential equations that are

24

either difficult or impossible to solve analytically. It entails a set of schemes or systems of algebraic equations that can be easily implemented computationally to arrive at reasonably accurate solutions to initial problems. The fundamental idea behind any finite difference scheme is related to the definition of the derivative of a smooth function at a point $x \in \mathbb{R}$ thus:

$$\dot{u}(x) = \lim_{h \to 0} \frac{u(x+h) - u(x)}{h} \tag{18}$$

Moreover, when h tends to 0, the right-hand side of the equation 18 above provides a good enough approximation of the derivative. That is, h should be small enough to give a good approximation of the derivative. We can use the equation 18 to discretize a partial differential equation (PDE) on a regular space grid of finite intervals of $x \in [0, L]$. This approximates $x \in [0, \infty)$. Within a rectangular mesh grid with points (t_n, x_j), we will have a fixed space step of Δx and a fixed time step of Δt on a regular time grid. The grid is such that:

$$0 = t_0 < t_1 < t_2 \dots, \qquad 0 = x_1 < x_2 < x_3 \dots < x_N = L \tag{19}$$

where

$$x_j = (j-1)\Delta x, \ \ t_n = n\Delta t, \ \ for \ j = 1, 2, 3, \dots, N, \ \ n = 0,1,2,3 \dots. \tag{20}$$

Rewriting the equation 18 using the grid indices, we have the following:

$$\frac{\partial u_j^n}{\partial t} = \frac{u_j^{n+1} - u_j^n}{\Delta t} + \vartheta(\Delta t) \tag{21}$$

where $\vartheta(\Delta t)$ is the truncation error. This is called the **forward difference**. Applying this knowledge to equation *16a*, we have the following discretization scheme for the next time step:

$$\boldsymbol{u}_{j+i}^n = \boldsymbol{u}_j^n + D\Delta t \left[\frac{\boldsymbol{u}_j^{n+1} - 2\boldsymbol{u}_j^n + \boldsymbol{u}_j^{n-1}}{\Delta x^2} \right] + \boldsymbol{f}(\boldsymbol{u}_j^n)\Delta t + \boldsymbol{I} \tag{22}$$

25

Below is a table of finite difference formulas for first and second order differential equations:

Order	Forward	Backwards	Center
First	$\dfrac{\partial u_j^n}{\partial t} = \dfrac{u_j^{n+1} - u_j^n}{\Delta t}$ $+ \vartheta(\Delta t)$	$\dfrac{\partial u_j^n}{\partial t} = \dfrac{u_j^n - u_j^{n+1}}{\Delta t}$ $+ \vartheta(\Delta t)$	$\dfrac{\partial u_j^n}{\partial t}$ $= \dfrac{u_j^{n+1} - u_j^{n-1}}{\Delta t}$ $+ \vartheta(\Delta t)$
Second	$\dfrac{\partial^2 u_j^n}{\partial t^2}$ $= \dfrac{u_j^{n+1} - 2u_j^{n+1} + u_j^n}{\Delta t^2}$ $+ \vartheta^2(\Delta t)$	$\dfrac{\partial^2 u_j^n}{\partial t^2}$ $= \dfrac{u_j^n - 2u_j^{n-1} + u_j^{n-2}}{\Delta t^2}$ $+ \vartheta^2(\Delta t)$	$\dfrac{\partial^2 u_j^n}{\partial t^2}$ $= \dfrac{u_j^{n+1} - 2u_j^n + u_j^{n-1}}{\Delta t^2}$ $+ \vartheta^2(\Delta t)$

Table 2: The table above shows the finite difference scheme for first and second order differential equations.

Goals

The central hypothesis of this research is that a computational one-dimensional reaction diffusion model with nonlinear diffusion may be used to investigate AP propagation in a PN and determine regimes for propagation entrainment in injured PN.

The specific goals of this dissertation are:

1. To model action potential (AP) propagation in 1D cable using reaction-diffusion equations with nonlinear diffusion and obtain conditions for stable propagation of AP propagation in a Peripheral Nerve (PN) with no excitability impairment.

2. To modify reaction-diffusion equations from aim 1 to model impaired AP propagation in injured PN and determine excitation wavetrains with shortest APD.

CHAPTER II: DEVELOPMENT AND ANALYSIS OF RD EQUATIONS FOR

DESCRIPTION OF NONLINEAR AP DIFFUSION IN A 1D PERIPHERAL NERVE (PN)

CABLE WITH UNIMPAIRED EXCITABILITY

Abstract

In this section, we study the effects of nonlinear diffusion on wave propagation generated in normal tissues using a one-dimensional Fitzhugh-Nagumo (FN) model. Changes in action potential duration (APD) and Repolarization interval (RI) are observed based upon modification of the FN model diffusion term by adding quadratic or quartic transmembrane potential dependent diffusion component. We determined that at the same values of RIs, the waves propagating in such excitable media had longer APDs and consequently were more stable than in the media with constant diffusion. Furthermore, it has been found that changes in the amplitudes of both types of a nonlinear diffusion term resulted in periodic oscillations of both APD and RI. We also determined that the propagating waves were more stable for the quadratic compared to a quartic case when a constant component of the diffusion was higher.

Introduction

Peripheral nerves (PNs) are an integral part of messaging in the human body. These messages are in the form of electrical impulses. PNs exist outside the brain, and the spinal cord and are responsible for relaying messages from the brain to other parts of the body and back. PNs are bundled into axons which are found throughout the body. Messages are received by the dendrites of the PN and travel down the axon to the cell body. Several types of diseases can

27

affect the peripheral nerves. Peripheral neuropathy is commonly seen. Different conditions in the

body cause it. These include but are not limited to diabetes, autoimmune disease, infections, and

many more. Some deficiencies or disorders in the body could also manifest as neuropathy in the

nerve. For example, in a teen with Riboflavin Transporter Deficiency, peripheral nerves are the

primary site of pathology[38]. This deficiency will manifest as motor, sensory and cranial

neuropathy. In this section, we are dealing with healthy PNs. We are interested in modeling

action potential propagation in PNs using a modified version of the FitzHugh Nagumo model.

This enables us to consider some significant factors, such as the significant charge depletions

that usually occur in PNs. This section will present a more holistic representation of the

propagation of action potential in PNs.

Method

Modelling of RD equations with nonlinear diffusion function to describe 1D geometry of the PN.

There are many different RD equations to describe excitability, and each has its

advantages. Entire articles and journals are dedicated to describing and showcasing some of

these equations. Charged ions aggregate on the nerve cells' membrane due to their capacitance.

In biological membranes, the resting potential depends mainly on the magnitude of these charges

and the membrane capacitance[39]. It is, therefore, reasonable to know how much intracellular or

extracellular concentrations of these ions are modified by this charge aggregation. To understand

this, we will need a measure of the relative charge depletion. It is well known that using sodium

and potassium 2-current model is well justified for AP propagation in large axons[40]. For axons

with large diameters, the amount of charge Q_m, moved through the axon during each action

potential is very small compared to intracellular ionic charge, Q_i. Thus, with a membrane capacitance C and an action potential amplitude U, we can estimate the relative charge depletion per 1cm of axonal length as:

$$\rho = \frac{Q_m}{Q_i} = \frac{2 \cdot 10^3 \cdot CU}{\alpha_M \cdot F_k \cdot r} \tag{23}$$

Where α_M, F_k and r are the extracellular sodium molar concentration, Faraday constant and axon radius, respectively. If we set the nominal values for these parameters as 20μF/cm², 150mV, 5mM/l with F_k = 9.65 x 10⁴C/mole, and axon radius of 1mm, then the value of ρ will be very small and thus negligible (ρ = 0.124 x 10⁻³). Under such conditions, there is no change between intracellular and extracellular *Na* concentration. However, in our case of small peripheral nerves (typically < 1.5mm in diameter), the significant charge depletion in the excitable cellular membrane must be considered. Therefore, we introduce a nonlinear diffusion coefficient, which depends on the amplitude of AP of the order:

$$D[u] = D_0 + \alpha(u^m) \tag{24}$$

To justify this introduction, we go back to Fick's laws of diffusion. According to classical Fick's law, the flux of *J* of any material (cells, chemical concentration, animal density, etc.) is proportional to the gradient of the concentration of the material. In our case where the action potential is *u*, Fick's law in one dimension is represented by:

$$J \propto -\frac{\partial u}{\partial x} = -D\frac{\partial u}{\partial x} \tag{25}$$

Where D is the diffusion constant. Note that the negative sign tells us that diffusion transports matter from a region of high concentration to a region of low concentration. If we write the general conservation equation, which says that the rate of change of amount in a region is the same as the rate of flow across the boundary added to any other that is created in the

boundary, then in such a region as $x_0 < x < x_1$ where no material is created, we have the following equation:

$$\frac{\partial}{\partial t}\int_{x_0}^{x_1} u[x,t]dx = J[x_0,t] - J[x_1,t]$$

(26)

Let us take $x_1 = x_0 + \Delta x$ and take limits as $\Delta x \to 0$. This results in the classical diffusion equation or Fick's second law in one dimension:

$$\frac{\partial u}{\partial t} = -\frac{\partial J}{\partial x} = \frac{\partial}{\partial x}\left(D[u]\frac{\partial u}{\partial x}\right)$$

(27)

D is **not** a constant diffusion.

In animal and insect dispersions studies, nonlinear diffusion models have also been used. One of such models is in a form with a diffusion coefficient dependent on population density n such that D increases with n. It is such that equation 27 above can be rewritten as:

$$J = -D[n]\nabla n, \qquad \frac{dD}{dn} > 0$$

(28)

A typical form that D takes is $D_0\left(\frac{n}{n_0}\right)^m$ where $m > 0$, D_0, n_0 are both positive constants[34].

Thus the dispersal equation in one dimension according to [34] is:

$$\frac{\partial n}{\partial t} = D_0\frac{\partial}{\partial x}\left(\frac{n}{n_0}\right)^m\frac{\partial n}{\partial x}$$

(29)

Where n_0 is a reference population. As $m \to 0$, $D[n] \to D_0 \to 1$. This shows that there is an increase in diffusion due to population pressure.

Insects with a low population frequently tend to aggregate. The following model reflects the flux of this aggregation:

$$J = U\,n - D[n]\frac{\partial n}{\partial x}$$

(30)

30

Where U is transport velocity, in our case, the diffusion of charges and action potential becomes significantly dependent on charge depletion from intracellular space. In this case, because of charge depletion, there is a similarity to the insect population density pressure scenario where a description of diffusion with a nonlinear term concerning population density is justified. Therefore, one can consider an analogous nonlinear term with respect to transmembrane potential. Indeed, an excessive (depleted) charge "pressure" is similar to the population density pressure. This is because $Na+$ and $K+$ charges that flow across the membrane potential are all positive, and their overconcentration in extracellular space creates an additional repulsive force, thus resulting in nonlinear diffusion. We, therefore, employ a similarity to this situation and introduce our nonlinear diffusion coefficient of the form in the FitzHugh-Nagumo model with a nonlinear diffusion coefficient shown in equations 31 below.

Within this research, we will try to strike a balance between simplicity and accuracy, as this is necessary to obtain a near accurate description of the 1D nerve cable. Therefore, this model explicitly includes the source amplitude A. The governing RD equations are described below.

$$\frac{\partial u}{\partial t} = D[u]\frac{\partial^2 u}{\partial x^2} - A(u - m_1)(u - m_2)(u - m_3) - v + I_{stim} \tag{31}$$

$$\frac{dv}{dt} = \varepsilon(\gamma u - v)$$

$$D[u] = D_0 + d(u^k)$$

$$I_{stim} = \delta[\theta(t) - \theta(t - \Delta)]$$

Function u characterizes transmembrane potential and v defines a slow recovery variable that provides a negative feedback [41]. Coefficients γ, d and D_0 are constant parameters, k is a positive integer. Constants m_1, m_2, and m_3 which determines the equilibria of the nonlinear

oscillatory system described by equations 31, were set to 0, 0.63 and 2.25 respectively and $k = 2$ or 4. Since diffusion everywhere should be positive, and action potential could be negative during the period, we keep only even powers in the expression of the nonlinear diffusion. Furthermore, we found it appropriate to choose the values of k to be either 2 or 4 as higher even powers show a further loss of stability. A source amplitude A (the cubic nullcline) was fixed at 2.0 with recovery rate coefficient given as $\gamma = 2.0$ and ε fixed initially to 0.005. An external electric current is denoted by I_{stim} where θ is the stepwise Heaviside function. The amplitude δ and the duration Δ of the external electric current are set to 0.5 and 0.2 respectively and are kept constant.

At end and the beginning of the 1D cable, Neumann boundary conditions were used. This means that the electric field or gradient across the boundary is set to zero, which allows the RD wave to pass through the boundary. This *"no-flux"* boundary is described below.

$$\frac{\partial u}{\partial n} = 0 \tag{32}$$

Where n is the normal to the channel boundary.

We have a 1D cable (simulating the Neuron) of finite length ($200\Delta x$) using a second order explicit difference scheme with zero flux boundary conditions in this experiment. Spatial Δx and temporal steps Δt used in the numerical integration were equal to 0.1 and 0.001 respectively. Special and temporal scales were set to $100\mu m$ and $1ms$ respectively to reflect the spatiotemporal dimensions of action potential propagation in a quite small trochlear nerve of $\sim 25mm$ in length [42,43]. D_0 and d were fixed at 0.08 and 0.001 respectively. ε was 0.005. The length of the cable was set to $200\ \Delta x$. To initiate an excitation wavetrain the excitation stimuli were periodically applied at the $x = 0$ end of the PN. Here and further, we will denote a period between successive stimuli as a basic cycle length BCL [44]. An example of such periodic

wavetrain computed using equation 31 based on the numerical method above is shown in Fig. 10.
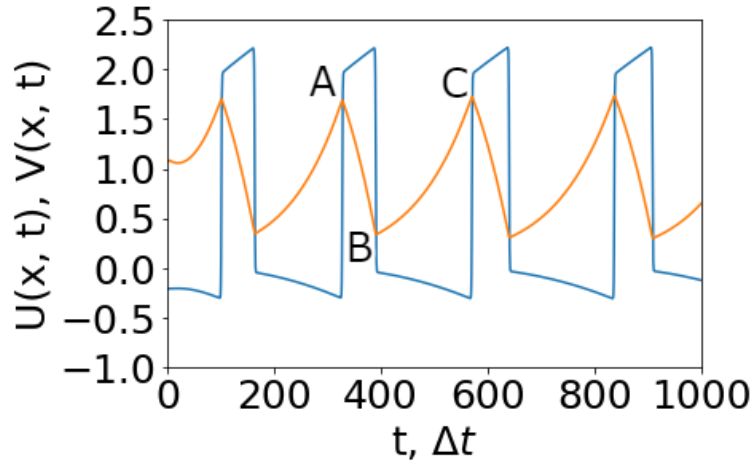
Figure 10 - Shows a steady state snapshot of the wave train computed using equations 32. AB shows the APD, and BC shows the RI.

The initial period of stimulations is equal to $600\Delta t$. After the wave resulted from the BCL stimulations reached a steady state at a certain distance from $x = 0$, the BCLs get shorter by $40\Delta t$ and stimulations continue until the next wave reaches a new steady state. All accumulated in this way steady state waves are characterized by APD responses which make up an important characteristic of PN known as a restitution curve [20].

Changes of APD values measured at the margin of wavetrain stability, near the end of the restitution curve (APD_{end}, BCL_{end}), play a vital role in the analysis of our numerical simulations. It is important to note here that the APD_{end} is the time duration of the final action potential when the propagation becomes so unstable that the PN fiber does not respond to more stimuli anymore. This point is characterized by tightly packed wavetrains. The same goes for the BCL_{end}. It is simply the sum of the final APD and final Repolarization Interval (RI), when the wavetrain becomes unstable and unresponsive to stimuli. When APD and BCL values get close to APD_{end} and BCL_{end} the propagation of the wavetrain becomes unstable, so the insufficiently recovered

33

PN fiber does not respond to the next stimulus and exhibits unstable M:N (M stimuli and N responses M≠N) wave patterns[45]. Figure 10 demonstrates a case for sufficiently short DIs causing the PN to stop responding to the next stimulus exhibiting M:N instability after reaching a steady state.

Results

Application of RD model for stabilization of excitation waves

We consider results of simulation of AP propagation in the intact PNs without injured portions. While we aim to understand the stability of excitation waves and dependence of the restitution curves $APD = F(DI)$ on the nonlinear part of the diffusion coefficient, we found that all components of nonlinear diffusion function play a significant role in the stabilization of propagation of excitation waves by effecting the restitution curves minimal values APD_{end} and RI_{end} measured at the ends of the curves.

Setting $\varepsilon = 0.005, 0.006$ and plotting the restitution curves for two conditions; (a) with no nonlinear component and (b) with the quadratic nonlinear component u^2 and coefficient $d = 0.02$. we have the following (Fig. 11):
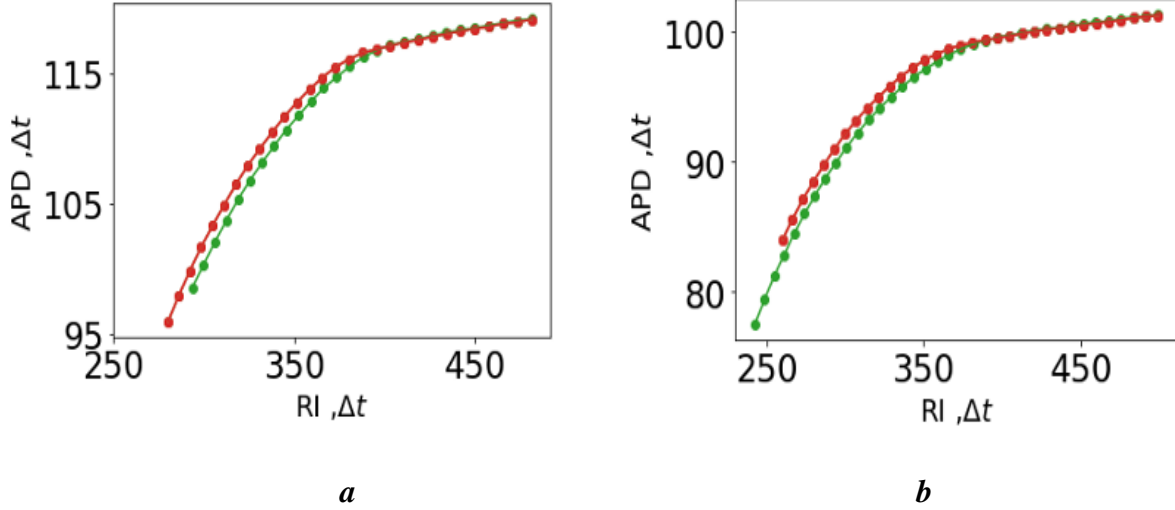
Figure 11 - Panels (a) and (b) show the restitution dependences measured at x=0.25L for ε = 0.005 (a) and ε = 0.006 (b), respectively. Dependencies for constant, $D(u, x) = 1$, and nonlinear, $D(u, x) = 1 + 0.02u^2$, diffusion are depicted by red and green dots, respectively. Smooth green and red curves are 5th order splines.

Fig. 11 demonstrates the differences between the ends of restitution curves (extent of stability of propagation) for different ε and different diffusion scenarios, including the cases with constant diffusion coefficient $d = 0$ and the quadratic nonlinear diffusion du^2 ($d = 0.02$). Fig. 11 also demonstrates that in both cases (linear and nonlinear) for the same RI the waves with nonlinear diffusion have slightly wider APDs. However, Fig. 11 also reveals that for the same RI the waves with non-linear diffusion have slightly shorter APDs. It should be noted that values of APD$_{end}$ and RI $_{end}$ strongly depends on ε and alternate such as at ε=0.005 (Fig.11a) the restitution curve with constant diffusion has a shorter APD$_{end}$, while at ε=0.006 (Fig. 11b) the situation is reversed.

To further quantify the effects of nonlinearity on the restitution characteristics, we fixed the linear diffusion coefficient D_0 at 0.8 while varying the nonlinear diffusion coefficient d from 0.02 to 0.05 in steps of .01. The same sequence was repeated for D_0=1.
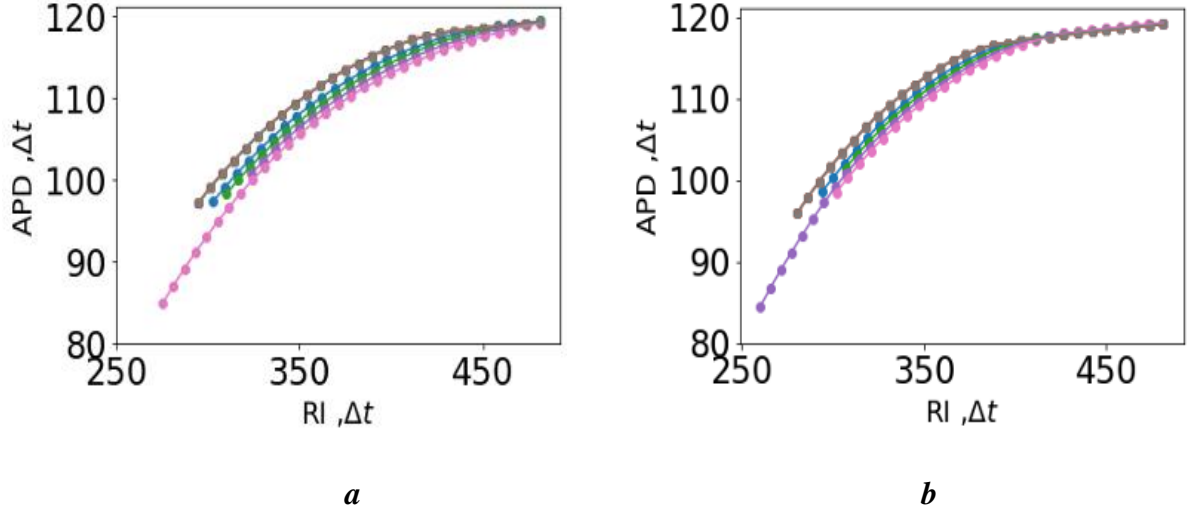
Figure 12 - Restitution dependences computed for different nonlinear diffusion functions $D(u, x) = 0.8 + d(u^2)$ (a) and $D(u, x) = 1.0 + d(u^2)$ (b). Both restitution dependences are measured at $x = 0.25L$. Gray, blue, green, purple, and pink color dots relate to $d = 0; 0.02; 0.03; 0.04; and 0.05$, respectively. Corresponding smooth color curves are 5th order splines.

Fig. 12 demonstrates a non-monotonous character of dependence of the APD$_{end}$ on the magnitude of the nonlinear diffusion coefficient d. At $D_0 = 0.8$ when d rises from 0.02 to 0.04, the corresponding APD$_{end}$ increase to the value exceeding 95 (Fig. 12a). However, when d gets higher, approaching 0.05, the corresponding APD$_{end}$ drops sharply to the level slightly above 85. At $D_0 = 1.0$ (Fig. 12b), the non-monotonous behavior of the APD$_{end}$ increases in intensity in such a way that APD$_{end}$ values oscillate up and down at each incremental shift of d.

In the next set of simulations, we continue to analyze restitution dependences and investigate specifics of BCL$_{end}$ and APD$_{end}$ changes with coefficients d and D_0 for $m = 2$ (quadratic) and $m = 4$ (quartic) cases in the Eq. (33) below:

$$D[u] = D_0 + d(u^k)$$

(33)

$$where\ k = 2\ and\ 4$$

36

We plotted the end behavior for the BCL$_{end}$ vs d. The values for the nonlinear coefficient d ranged from 0.0 to 0.1 in increments of 0.01.
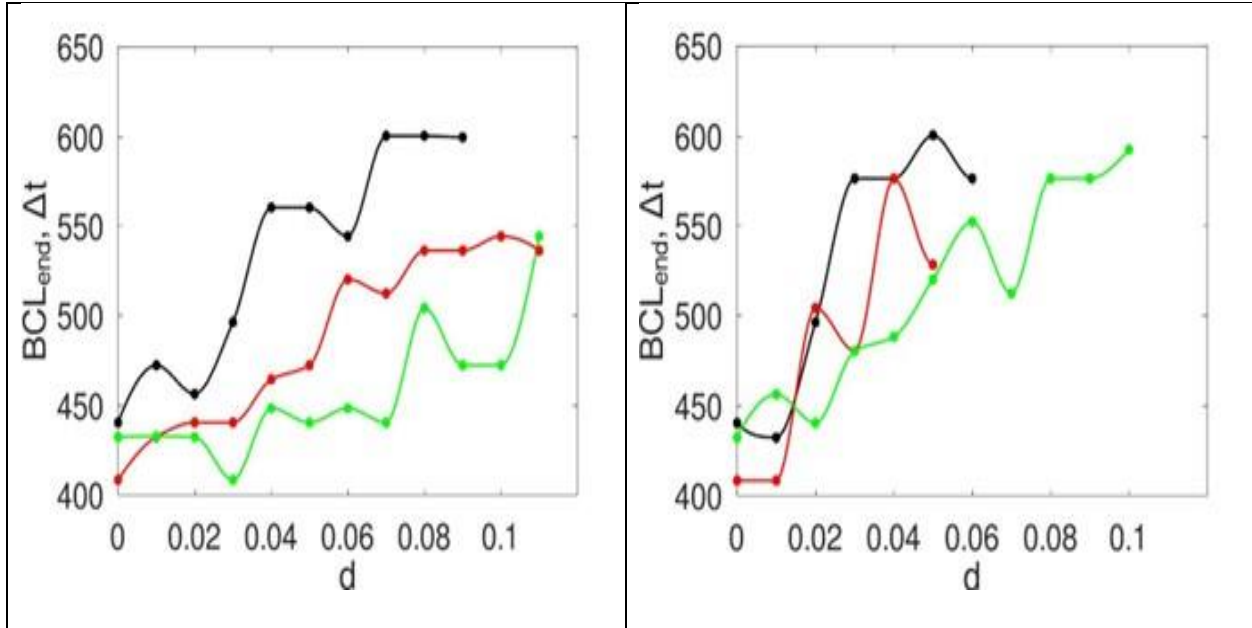
Figure 13 - Dependences of BCL_{end} on d ($x = 1.25L$) for $D_0 = 0.4$ (black), $D_0 = 0.5$ (red) and $D_0 = 0.6$ (green) in quadratic ($k = 2$) (panel a) and quartic ($k = 4$) (panel b) models of nonlinear diffusion (Eqs. 2). Corresponding smooth color curves are 5th order splines.

Dependences of BCL$_{end}$ in Fig. 13 show oscillations of BCL_{end} vs. d which occur in a wide range $0 < d < 0.1$ with slightly higher frequencies for the quartic nonlinear diffusion. It is of notice that, unlike quadratic case where BCL$_{end}$ oscillations are stable within practically a whole range of d for all values of D_0, in the quartic case, stable propagation of excitation waves for greater values of $d > 0.06$ is present only at $D_0 = 0.6$ (Fig. 13b). Overall, observed BCL$_{end}$ oscillations evolve in the way that corresponding trends with respect to d are positive (Fig. 13).
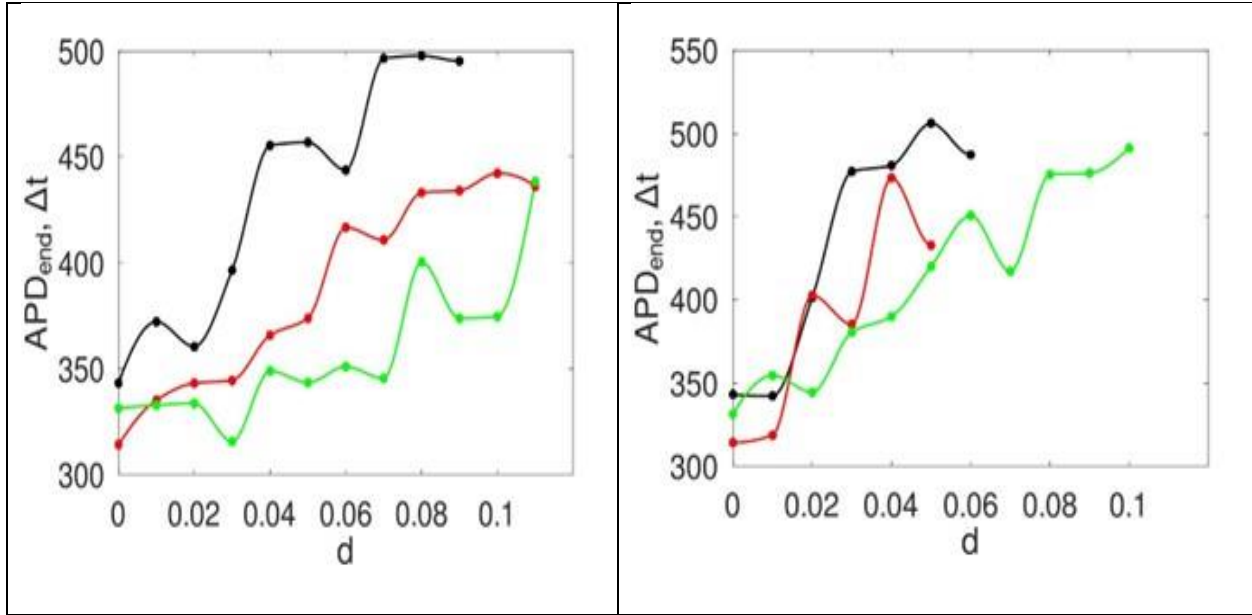
Figure 14 - Dependences of APDend on d (x=1.25L) for D_0= 0.4 (black), D_0= 0.5 (red) and D_0= 0.6 (green) in quadratic (panel a, k = 2) and quartic (panel b, k = 4) models of nonlinear diffusion (Equations 2). Corresponding smooth color curves are 5th order splines.

We determined that dependences of APDend are also oscillatory and have an overall positive trend versus parameter *d*. However, the amplitudes of these oscillations are smaller than those for the BCLend, especially in the quartic case. Similar to BCLend shown in Fig. 13, the values of APDend decrease for greater D_0, particularly in the quartic case.

Discussion

We demonstrated that using a one-dimensional Fitzhugh-Nagumo model with nonlinear diffusion we can successfully simulate the propagation of electrical pulses through healthy nerves. We noticed that APDend values are shorter for nonlinear diffusion case at $\varepsilon = 0.005$,

although for linear diffusion at $\varepsilon = 0.006$ we observed the opposite. This indicates that ε significantly affects stability of AP wavetrains allowing them to propagate with shorter periods depending on value of this parameter.

Conclusion

We implemented a one-dimensional Fitzhugh-Nagumo model to simulate the propagation of electrical excitation in healthy nerves. The model was modified to account for effects of an action potential nonlinear diffusion evolving due to a significant intracellular charge depletion associated with a small size of peripheral nerves. We have found that the nonlinear diffusion plays a critical role in the stabilization of propagation in healthy nerves. Specifically, we established that reduction in amplitude of nonlinear diffusion term in healthy PNs stabilized excitation, so AP wavetrains were able to propagate through the cable at substantially shorter *BCL*s incrementally decreasing at smaller values of ε.

CHAPTER III: DEVELOPMENT AND ANALYSIS OF RD MODEL TO DESCRIBE
APPROPAGATION IN PN WITH IMPAIRED EXCITABILITY

Abstract

In this section we continue to implement the one-dimensional Fitzhugh-Nagumo model.
We further modified the FN model from the previous section (CHAPTER II) to include diffusive
inhomogeneity in order to model conduction related injury in peripheral nerves. Our aim is to
understand the mechanism of stabilization of action potential propagation in injured nerves. We
investigated and compared AP propagation in normal and injured peripheral nerves of different
lengths with varied extension of diffusive injury. We argue that results of our numerical
simulations may help to gain some understanding of certain electrical conduction related neuro-
pathological phenomena like numbness and tingling and, therefore, assist in identifying potential
therapeutic targets.

Introduction

Peripheral nerve injuries (PNIs) remain an important health problem often leading to loss
of motor function, sensory function, or a combination of both in young and old people. It could
lead to various challenges to patients ranging from mild discomfort to life-long impairments[13].
PNIs are quite common in the United States and around the world presenting a wide range of
symptoms depending on how severe it is or what kinds of nerves are involved[46–48]. In Europe for
example, PNIs occur at a rate of about 300,000 new cases per year[49]. While not life-threatening,
PNIs can lead to a significant decline in a patient's quality of life. PNIs can be because of

accidents or traumas. This types of accidents or traumas could lead to a minor injury or in severe cases a fully severed nerve. When this occurs, the body naturally tries a peripheral nerve regeneration. Unlike what is observed in other tissues in the body, peripheral nerve injury regeneration is often slow and incomplete when it occurs. In most cases, surgical repair procedures with gene therapy are combined to enhance recovery after nerve damage. This clinical procedure involves the apposition and suturing of the two nerve ends without creating tension. Even after this end-to-end surgical nerve repair by suture, functional recovery has been quite disappointing due to a lack of selectivity and other factors. While there are a lot of resources published on the mechanism of injury and regeneration, not much progress has been made on treatments that leads to full recovery[13]. Many peripheral nerve injuries usually require surgical nerve reconstruction. Recovery of motor and sensory functions after a peripheral nerve injury is subpar even after a surgical procedure to repair damage. A meta-analysis of median and ulnar nerve repairs in 2005 demonstrated that only 52.6% achieve satisfactory motor recovery with even less 42.6% experiencing satisfactory sensory recovery[50]. This is as a result of the slow rate of axonal elongation during regeneration and atrophic changes that occur in denervated Schwann cells and target muscles with proximal lesions[2].

Anatomy and physiology of Peripheral Nerve Injury

Even with recent technological advances, the management of peripheral nerve injury (PNI) is still a major challenge in medicine. Managing PNI effectively is contingent upon a detailed understanding of peripheral nerve anatomy. After an injury to a peripheral nerve, there are some complex pathophysiological changes that occur at the site of injury. These changes include morphologic and metabolic changes. Changes are not limited to only the site of injury but can also be observed in the nerve cell body, in the segments proximal and distal to the site of

41

the injury and in the distal endings of both muscle endplates and sensory receptors. Changes can

first be noticed in nerve's cell body as early as several hours after the injury has occurred when

the axons begin to develop into several regenerating axons. Some of these changes, which are

morphologic in nature, are called chromatolysis. Chromatolysis involves cell body and nucleolar

swelling, and nuclear eccentricity. Metabolic changes can also be observed within the neuron.

These changes involve the synthesis of RNA, protein components, and lipids, as well as an

increase in glucose-6-phosphate dehydrogenase and hydrolytic enzyme production[51]. As we have

earlier stated, the primary responsibility of peripheral nerves is to transmit signals between the

spinal cord and other parts of the body. However due to these alterations of its metabolic

machinery as a result of injury, the peripheral nerve shifts away from this primary responsibility

and thus takes up the task of fabricating structural components for reconstructing of its injured

portion[52,53]. During the body's natural attempt at reconstruction after a peripheral nerve injury,

Schwann cells will begin processes that serve as physical guide to direct axons to their target.

Recent investigation shows that the rate of axonal regeneration is limited by the extension of

Schwann cells processes as against what was previously believed – axonal growth[54].

Classifications of Nerve Injuries

There are two different categories of classification for nerve injury – the Seddon and

Sunderland classifications of nerve injury. A classification scheme is important because it

enables physicians and scientists communicate about nerve pathophysiology in a common

language that is generally understandable. Seddon first classified nerve injuries into three

categories based on the presence of demyelination and severity of damage to the axons and the

connective tissues of the nerve[13,55]. Based on severity, Seddon classified nerve injuries into three

42

main categories: neurapraxia, axonotmesis and neurotmesis. Neurapraxia, which is the mildest of them, does not involve nerve discontinuity. It only leads to a transient functional loss. The transience of functional loss in neurapraxia is thought to be due to a local ion-induced conduction block at the injury site, even though subtle alterations in myelin structure have also been observed[56]. When axonotmesis occurs, there is a complete discontinuity of the nerve axons and the surrounding myelin structure. However, the surrounding mesenchymal structures, including the perineurium and epineurium are left intact. Neurotmesis is the most severe case. This involves a complete severance of a nerve. In this case, functional loss is complete and there will be no recovery without surgery. This is because of scar formation and the loss of mesenchymal guide which normally directs axonal regrowth. Sunderland on the other hand, further classified these three Seddon nerve injury description into five categories/degrees based on their severity[57]. A first-degree injury in Sunderland's description is equivalent to Seddon's neurapraxia while Sunderland's second degree is equivalent to Seddon's axonotmesis. Sunderland's third degree is placed between Seddon's axonotmesis and neurotmesis. This is because in the third-degree nerve injury, there is a severance of the axon and a partial injury to the endoneurium. Thus, depending on how severe the endoneurial damage is, functional recovery might be possible. Seddon's neurotmesis is further divided into two different degrees by Sunderland; fourth- and fifth-degree injuries. When there is a fourth-degree injury, all parts of the nerve are severed except the epineurium. Therefore, recovery is impossible without surgical help. The fifth-degree Sunderland's classification also involves a complete severance of the nerve. Likewise, recovery is not possible without surgical intervention. The figure below illustrates the comparison of both grading systems.
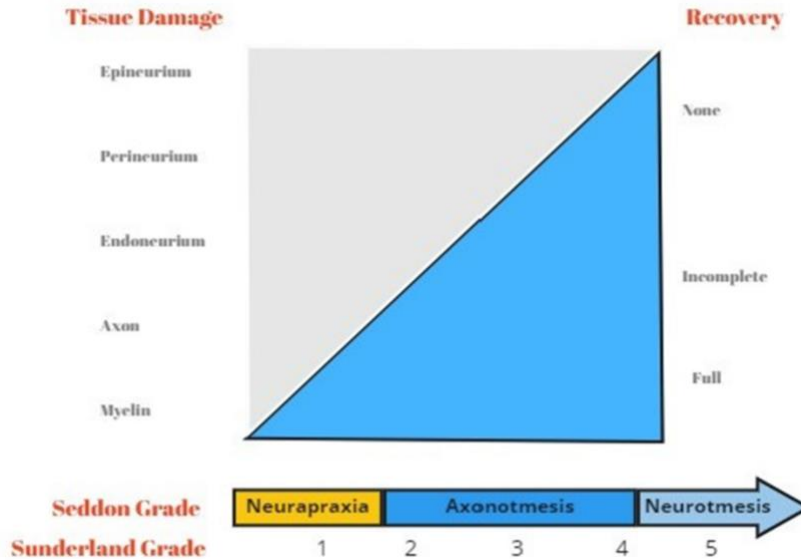
Figure 15 - Gradation in both the Sunderland and Seddon systems of nerve injury classification. This figure was adopted from [56]

The image in figure 16 below shows a visual representation of a comparison of both styles of classification of nerve injury. There have been several attempts to simplify these schemes even further by classifying nerves as either degenerative or nondegenerative. Significant among them is the method proposed by Thomas and Holdroff[58]. However, this has not been widely accepted.
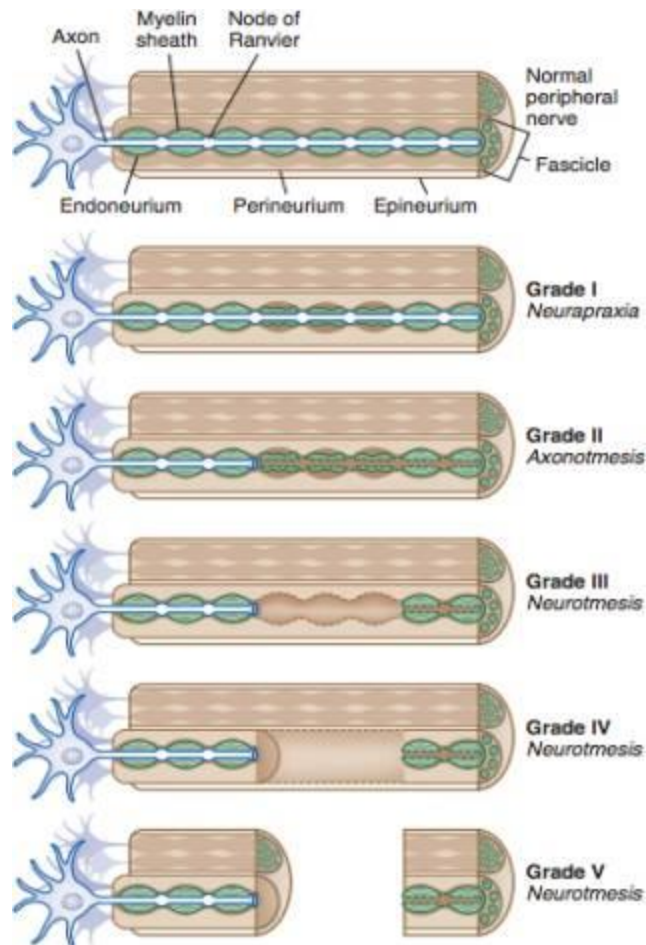
Figure 16 - Visual classification of nerve trauma[13]

Current techniques in nerve injury treatment

Peripheral nerve injuries are quite a common encounter in clinical practice. As we stated earlier, there are classifications of nerve injuries (Sutherland's and Seddon's) where natural rejuvenation and recovery is not possible. Surgical intervention is key to recovery. Here we discuss some of these surgical methods that have been developed to repair damaged peripheral nerves.

Direct Nerve Repair

Direct nerve repair involves a direct apposition of the two close and damaged ends of a peripheral nerve with the aim of suturing both ends together. This is recommended only when the two nerve ends to be sewn together can be held by a single 8-0 suture (0.04mm) with little to no tension[59]. Under this method of direct nerve repair are three techniques namely epineural repair, perineural repair and group repair. Epineural repair, which is the conventional technique for suturing lacerated nerves, involves aligning the nerve ends and placing sutures through the epineurium only[60–62]. It has the advantage of short operating time and a relative ease of the surgical procedure. Perineural repair is a technique of nerve repair that is used only when the repair involves 5 fascicles or less. The technique involves repairing individual fascicles and placing sutures through the perineurium[60]. Group repair is a technique that is used at an injury site where the nerves branch out such that fascicles are grouped.

Nerve Graft

A nerve graft is a piece of nerve whose extraneural support tissues will align and guide the outgrowth of axons from the proximal stum of a discontinuous nerve towards its target[63]. Nerve graft surgery is appropriate when the gap between damaged nerve ends is greater than 2cm and there is an extensive loss of nerve tissue. Nerve graft is the method of choice when direct end-to-end suturing is impossible[64]. Three common types of nerve graft are cable graft, trunk graft and vascularized nerve graft[62].

Nerve transfers

In nerve transfers, also referred to as neurotization, a proximal and functioning nerve which serves as a donor is used to repair the distal denerved nerve. In other words, either a healthy but less valuable nerve or its proximal stump is transferred with the aim that it innervates

a more important sensory or motor territory that has lost its innervation as a result of irreparable damage to its nerve[65]

Even with these surgical repairs and interventions, recovery rate is not encouraging. A recent study involving 51 patients over a 15-year period (2006-2020) showed that only approximately 42% of patients recovered to useful functional state after surgical treatment of nerve injuries[66].

To improve these outcomes, one needs to better comprehend pathophysiological features of the injured PN's electrical conduction which are currently insufficiently understood. In the following section, we will focus on numerical simulations of such features and determine the most stable regimes of propagation of electrical excitation characterized by shortest AP wavetrains.

Method

RD equations with nonlinear diffusion which model propagation of excitation in 1D PN with injury described by zones of impaired electrical conduction.

In this section, we are considering a grade III injury according to the Sutherland classification. This means that the axon is completely severed and there is an extensive damage to the endoneurium. In this case, there is a partial conduction block both proximally and distally and spontaneous recovery while possible, is difficult. To model and describe the propagation of excitations in small peripheral nerves with this level of injury, we modified the model from the previous chapter by considering an excitable cable with an area of inhomogeneous diffusion. The equation below describes this inhomogeneity mathematically:

$$\frac{\partial u}{\partial t} = D[u]\frac{\partial^2 u}{\partial x^2} - A(u - m_1)(u - m_2)(u - m_3) - v + I_{stim} \tag{34}$$

$$\frac{dv}{dt} = \varepsilon(\gamma u - v)$$

$$D[u] = D_0 + d^s[x](u^2)$$

$$d^s(x) = -0.5\beta[\tanh(3(x - L + \alpha)) - \tanh(3(x - L - \alpha))]$$

$$I_{stim}^{inj} = I_{stim} + I_{add}$$

The width of the injury zone is controlled by parameter α. The higher the value of α, the wider

the injury profile. Everything here will be considered in the case of quadratic diffusion term.

Without restriction of generality, we placed the inhomogeneity at the center of the cable and

extended the previous cable twice as much. We also displaced the inhomogeneity towards the

end of the cable and compared results. The figure 17 below shows a cable with the injury zone

positioned in the middle of the cable where diffusion is varied according to α.
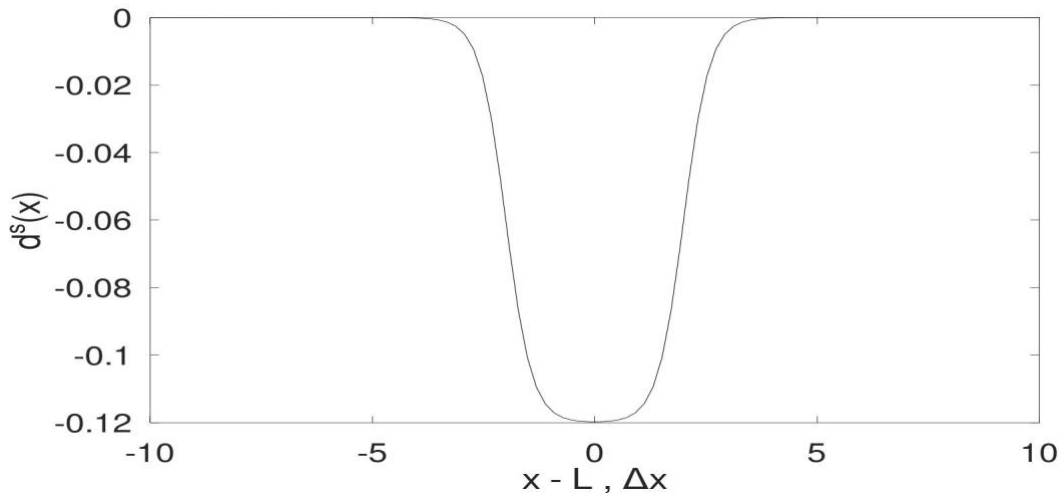
Figure 17 - Excitable cable with inhomogeneous diffusion injury profile ds(x) described by equations 35. $\alpha = 2.0$, $\beta = 0.18$ $L = 200\Delta x$. Inhomogeneous injury is located at the center of the cable.

Results

48

Initiation of wavetrains of excitation in injured PN

The system of Equations 34 produces a variety of solutions in response to periodic stimulations of injured PNs. Since injured PNs have reduced ionic conductance, the propagation of excitation wavetrains in the areas of injury can get destabilized. Under these conditions one needs to apply a stronger than without injury initial stimulus $I_{stim}^{inj} > I_{stim}$ (Equations 34) to initiate the propagation of excitation.

The stimulation I_{stim}^{inj} has been applied periodically (BCL=$200\Delta t$) at $x = 0$ end of the injured PN. The main part of the stimulus had the same as in the system of equations 31; amplitude equal to 0.5. To secure stable propagation of the excitation wavetrain throughout the whole injured cable, the additional shifted in time ($\Delta T = 60\Delta t$) stimuli I_{add} of the 3% amplitude of primary currents were applied at the same BCL at the same end of the cable.

Dependences of BCL_end on D_0 for nonlinear quadratic diffusion at different values of amplitudes in injured PNs and with injury at the center of the cable

In this section we do not change the amplitude of the coefficient of nonlinear diffusion, so parameter β in Equations 34 is constant. Instead, we alter the magnitude of D_0 and observe changes in BCL_end in response to variations of D_0 (Fig. 18).

49
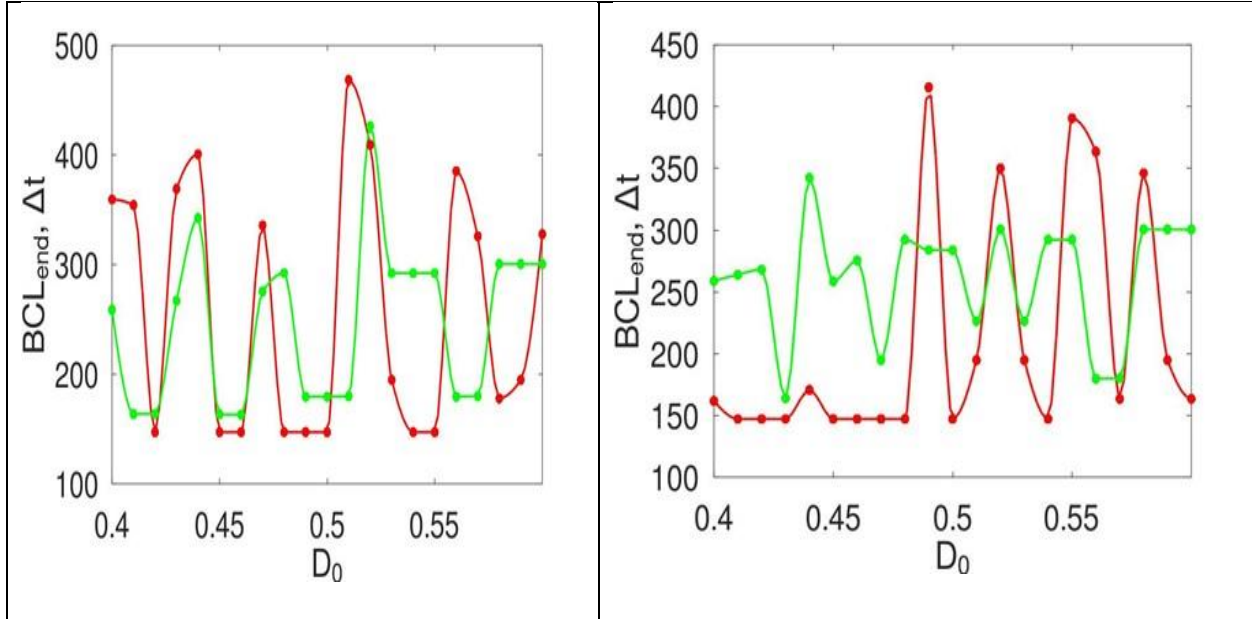
Figure 18 - Dependence of BCL$_{end}$ on D_0 with injury located at the center of the PNs. Panels (a), (b) are computed for α = 7 and 2, respectively. The green and red lines in both panels relate to L= 200Δx and L= 400Δx, respectively. δ= 0.45 and β = 0.12.

Figure 18a demonstrates that for longer injury (α = 7) oscillatory behavior of BCL$_{end}$ is practically synchronous in the lower range of D_0 < 0.5. However, for values of D_0 greater than 0.5 the phases of BCL$_{end}$ oscillations gradually diverge suggesting a decline of resonant diffusion patterns. These patterns considerably alter for shorter injury regions (α = 2) as synchronous oscillations, unlike figure 18a, appear only at D_0 > 0.5 (figure 18b). It should be noted that regardless of the injury's spatial extension the amplitude of BCL$_{end}$ oscillations for longer PNs is noticeably higher compared to PNs of shorter length.

Comparison of dependences of BCL$_{end}$ on D$_0$ for nonlinear quadratic diffusion at different values of cable lengths in injured PNs and with injury at the end of the cable.
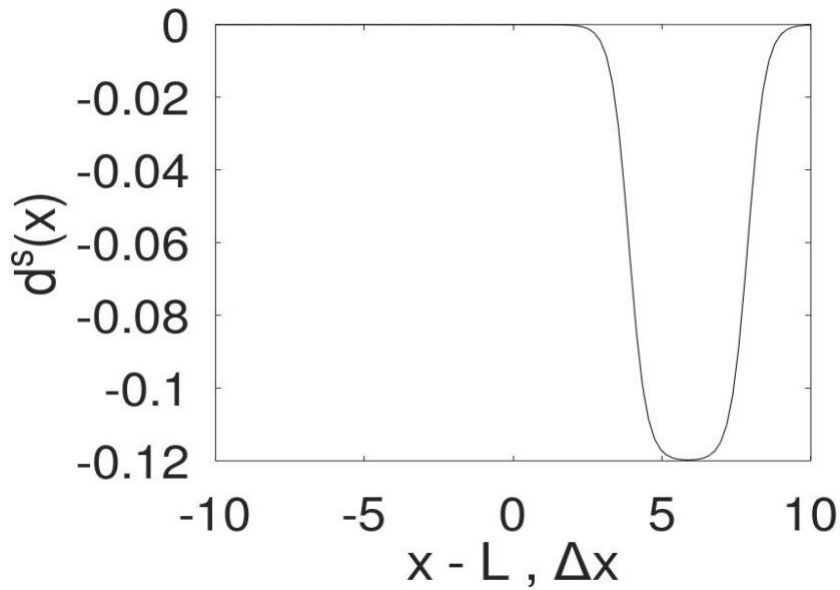
Figure 19 - Excitable cable with inhomogeneous diffusion injury profile ds(x) described by equations 35. α =2.0, β = 0.18 L = 200Δx. Inhomogeneous injury at the end of the cable.

In this section we also do not change the amplitude of the coefficient of nonlinear diffusion, so parameter β in Equations 34 remains intact. Instead, we alter the magnitude of D_0 and observe changes in BCL$_{end}$ in response to variations of D$_0$ and compare with different injury locations (middle of the cable and end of the cable) for various lengths (200Δx and 400Δx)
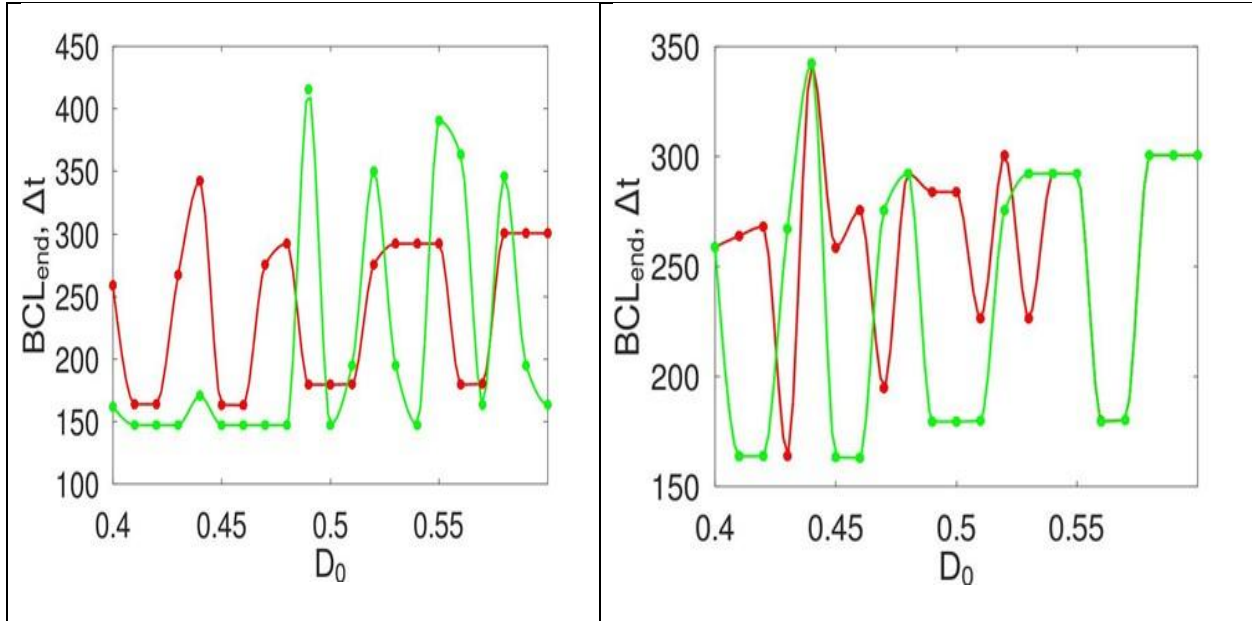
Figure 20 - Dependence of BCL$_{end}$ on D_0 with injury located at both the center (red) and end (green) of the PNs. Panels (a), (b) are computed for lengths $200\Delta x$ and $400\Delta x$ respectively. In both cases α = 2, δ= 0.45 and β = 0.12.

The Fig. 20a demonstrates that for injuries located at the center and at the end of the PN of shorter length, oscillatory behavior of BCL$_{end}$ is synchronous in the higher range of $D_0 > 0.5$. However, for values of D_0 less than 0.5 the phases of BCL$_{end}$ oscillations gradually diverge suggesting a decline of resonant diffusion patterns. Further, for longer PNs there was completely no synchronicity of BCL$_{end}$ vs D_0 oscillations between the cases when injury was located at the end and at the center of PN.

The Evolution of action potential in longer cable length with injury at the center of the cable.

In order to reveal the mechanism of BCL$_{end}$ oscillations in injured PNs we studied the D_0 dependent spatiotemporal evolution of AP waves in longer PN shown in Fig. 21-23.
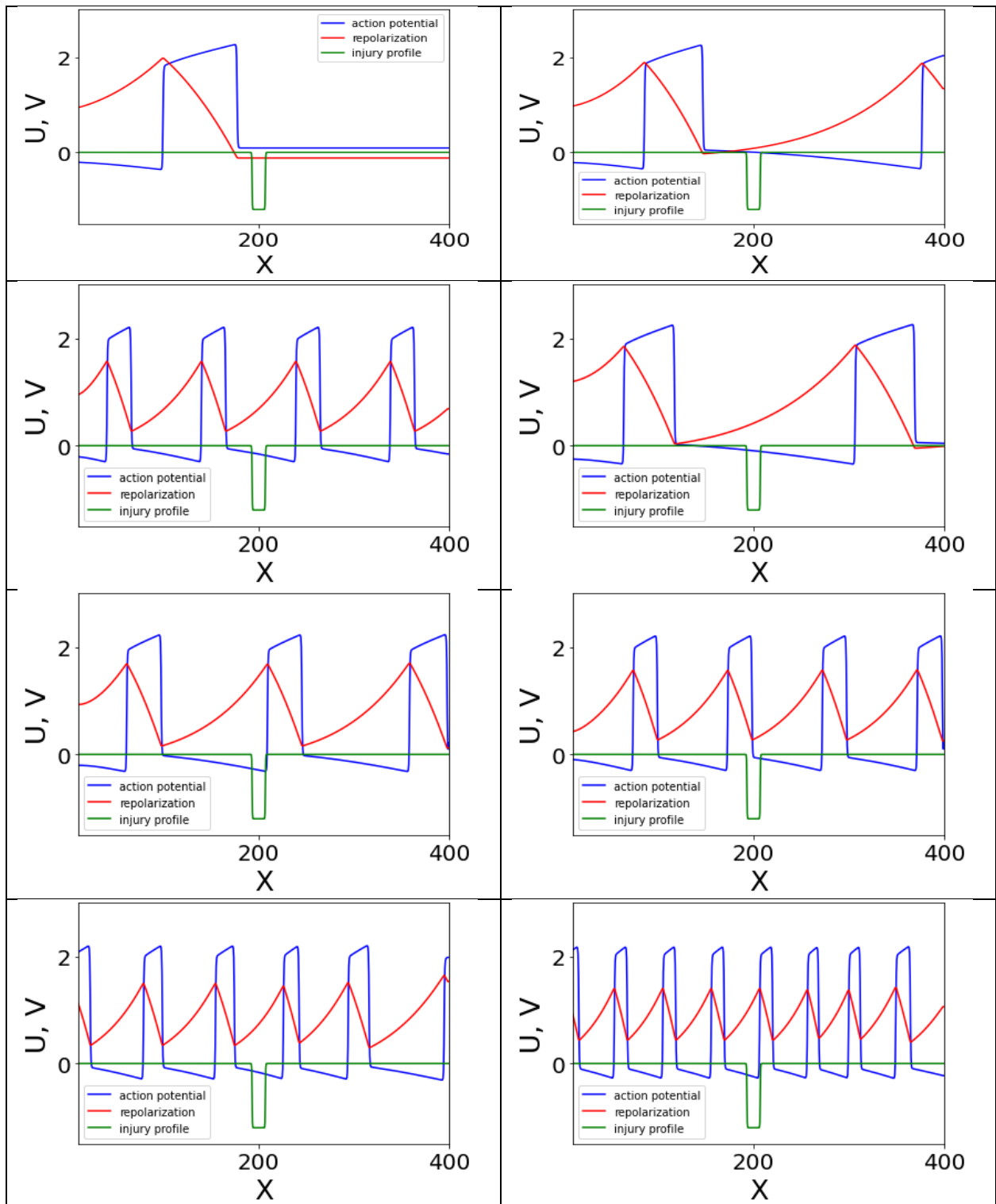
Figure 21 - Spatiotemporal evolution of action potential (blue curve) in PN with injury located at its center shown in green. Red curve is a recovery variable. This evolution is determined at PN stimulations period equal to BCL$_{end}$ for $\alpha = 7.0$, $D_0 = 0.49$, $\delta = 0.45$ and $\beta = 0.12$. The length of the cable is $400\Delta x$, time distance between snapshots is $28\Delta t$, time for the upper left panel snapshot is $6\Delta t$.
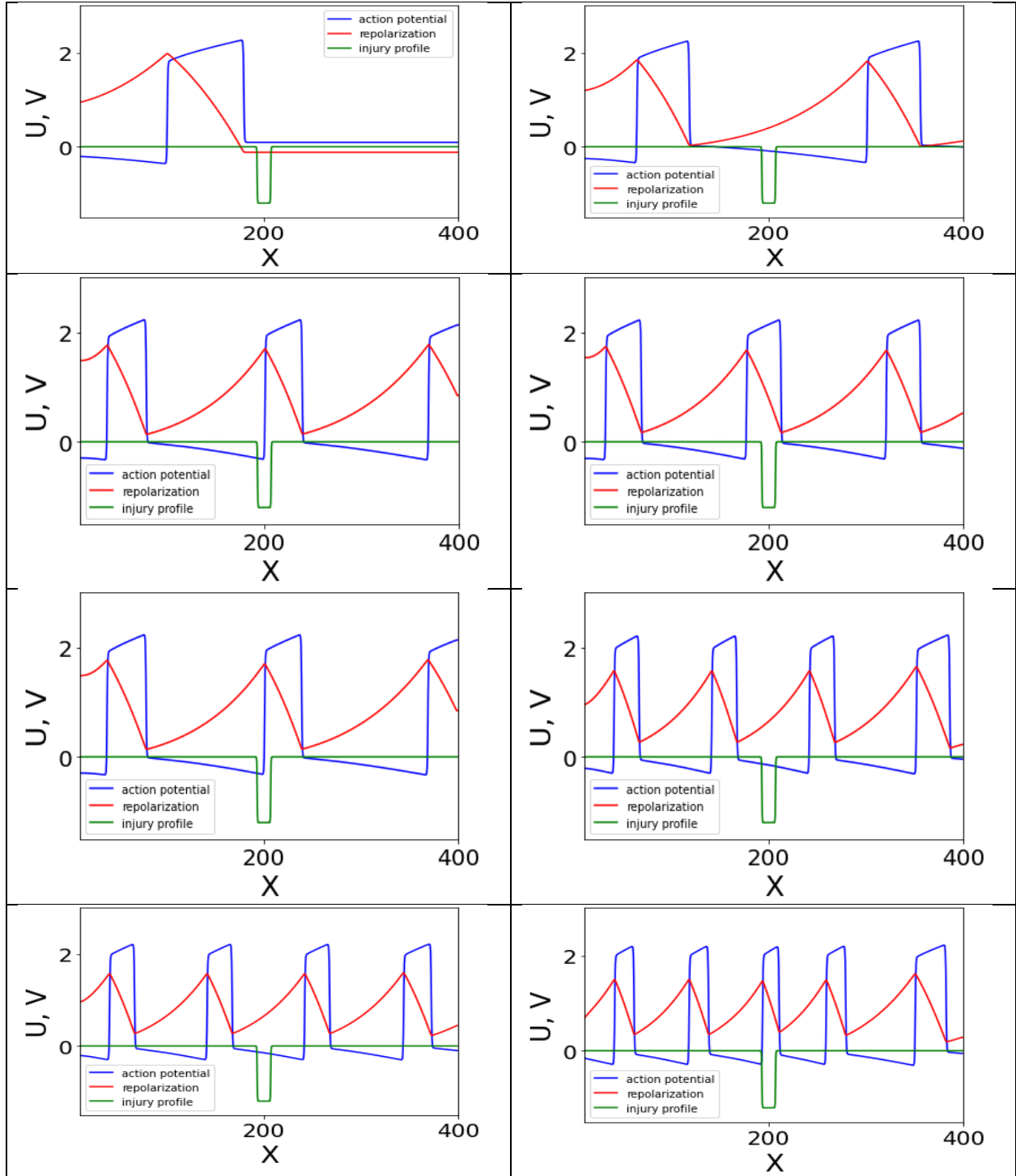
Figure 22 - Spatiotemporal evolution of action potential (blue curve) in a PN with injury located at its center shown in green. Red curve is a recovery variable. The evolution is determined at PN simulations period equal to BCL$_{end}$ for $\alpha = 7.0$, $D_0 = 0.5$, $\delta = 0.45$ and $\beta = 0.12$. The length of the cable is $400\Delta x$, time distance between snapshots is $20\Delta t$, time for the upper left panel snapshot is $5\Delta t$.

54
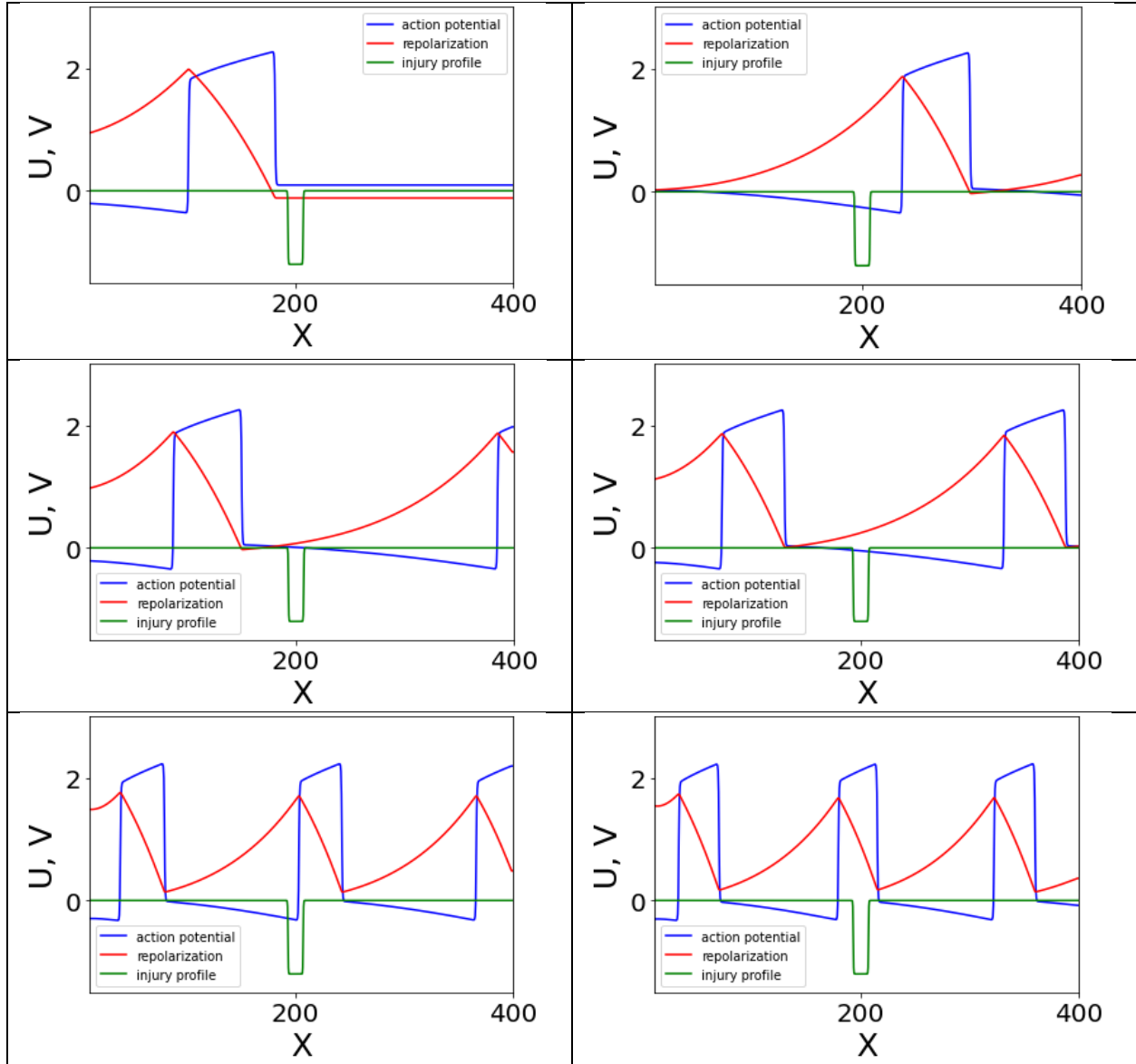
Figure 23 - Spatiotemporal evolution of action potential (blue curve) in a PN with injury located at its center shown in green. Red curve is a recovery variable. The evolution is determined at PN simulations period equal to BCL$_{end}$ for α = 7.0, D_0 = 0.51, δ = 0.45 and β = 0.12. The length of the cable is 400Δx, time distance between snapshots is 17Δt, time for the upper left snapshot is 6Δt.

As depicted in figures 21-23 periodic stimuli applied at the left ends of the injured PNs

initiate the propagation of AP waves with length and speed increasing for greater values of D_0.

The AP waves gradually evolve in time until they reach entirely developed steady state regimes

with progressively shortening periods of time $T_{F(21)} = 224\Delta t$, $T_{F(22)} = 160\Delta t$ and $T_{F(23)} = 102\Delta t$ as shown in figures 21, 22 and 23, respectively.

To allow additional waves to be inserted after each successive stimulation applied at PN's left end, the corresponding duration of BCL_{end} should be shorter than any of mentioned above values of $T_{F(i)}$. Fig. 21 and 22 show AP evolutions when this condition is met, so both T_{F22} and T_{F23} are greater than $BCL_{end} = 152\Delta t$ depicted in Fig. 18a ($D_0 = 0.49 - 0.5$, red curve).

However, when D_0 increases further to 0.51 (Fig. 23) the speed and spatial dimensions of the AP wave rapidly increase to the level sufficient to prevent multiple wave insertions. Indeed, a really wide steady state AP wave forms just within a short period of time ($T_{F(23)} = 102\Delta t$) after only two wave insertions resulting in much greater value of $BCL_{end} = 474\Delta t$.

Further growth of D_0 establishes conditions when only one AP wave can propagate in PN. When this wave approaches to the right end of PN, repolarization variable, v, is almost at the level of equilibrium, so multiple wave insertions shown in Fig. 21 and 22 may occur again, thus ensuring subsequent shortening of BCL_{end} and continuation of BCL_{end} oscillations.

Evolution of action potential in longer PN with injury located at the end of the PN.

We further studied the D_0 dependent spatiotemporal evolution of AP waves in PN of length $400\Delta x$ but with injury located at the end of the PN (Fig. 24 - 26).
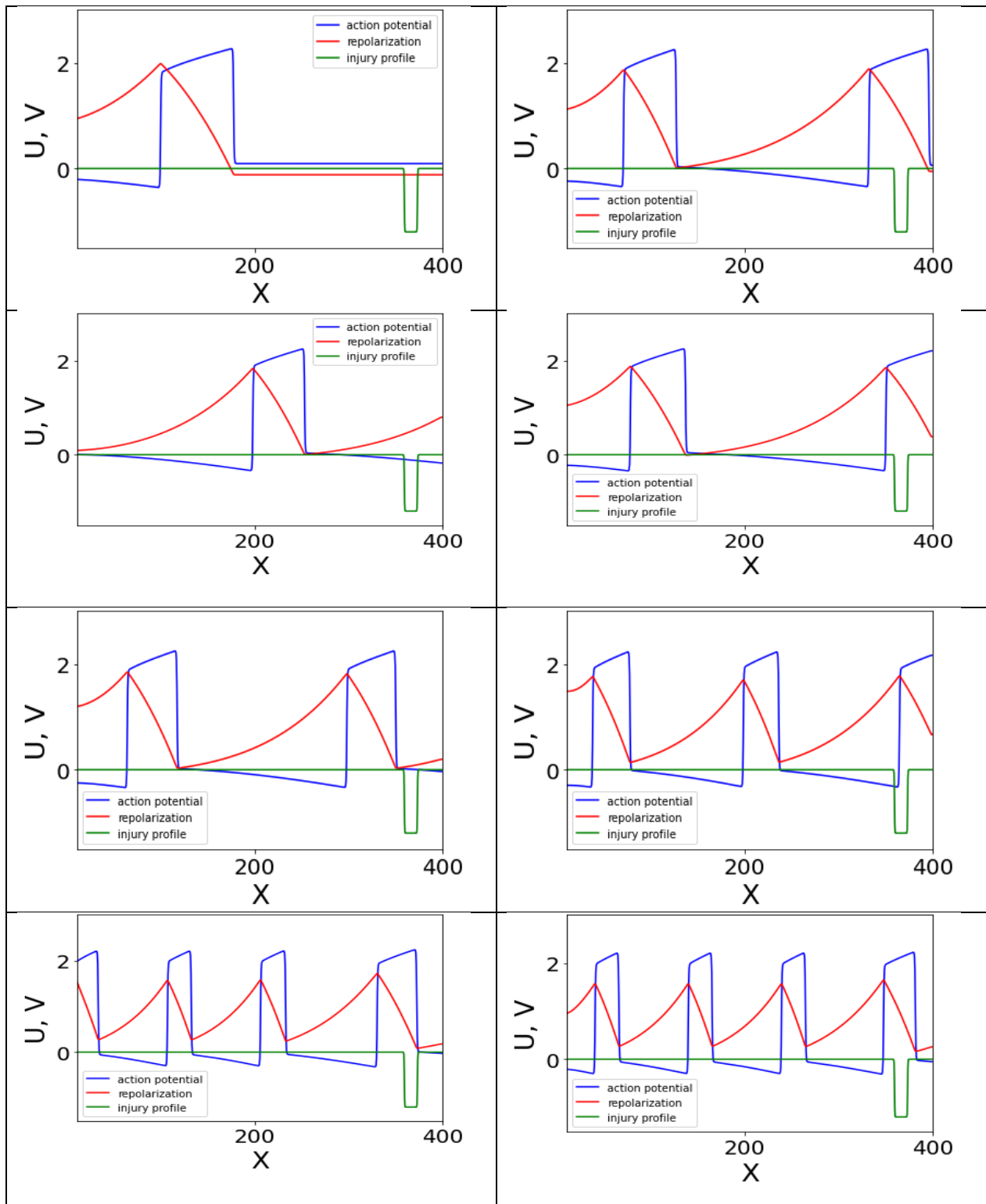
Figure 24 - Spatiotemporal evolution of action potential (blue curve) in PN with injury located at the end of cable shown in green. Red curve is a recovery variable. This evolution is determined at PN stimulations period equal to BCL$_{end}$ for $\alpha = 7.0$, $D_0 = 0.49$, $\delta = 0.45$. The length of the cable is set at the value of $400\Delta x$, time distance between snapshots is $12\Delta t$, time for the upper left snapshot is $6\Delta t$.
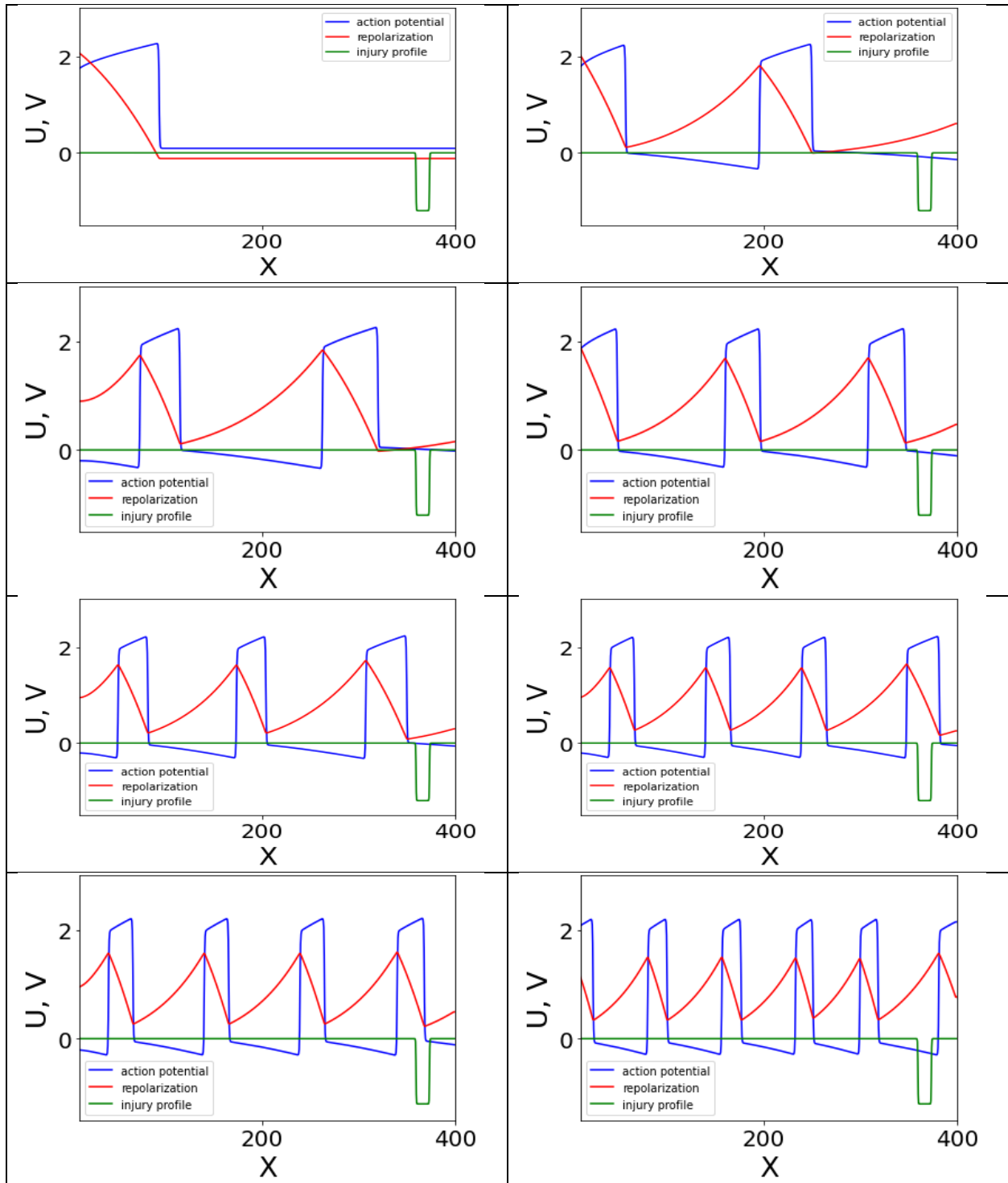
Figure 25 - Spatiotemporal evolution of action potential (blue curve) in PN with injury located at the end of cable shown in green. Red curve is a recovery variable. This evolution is determined at PN stimulations period equal to BCL$_{end}$ for $\alpha = 7.0$, $D_0 = 0.50$, $\delta = 0.45$. The length of the cable is set at the value of $400\Delta x$, time distance between snapshots is $18\Delta t$, time for the upper left snapshot is $4\Delta t$.

58
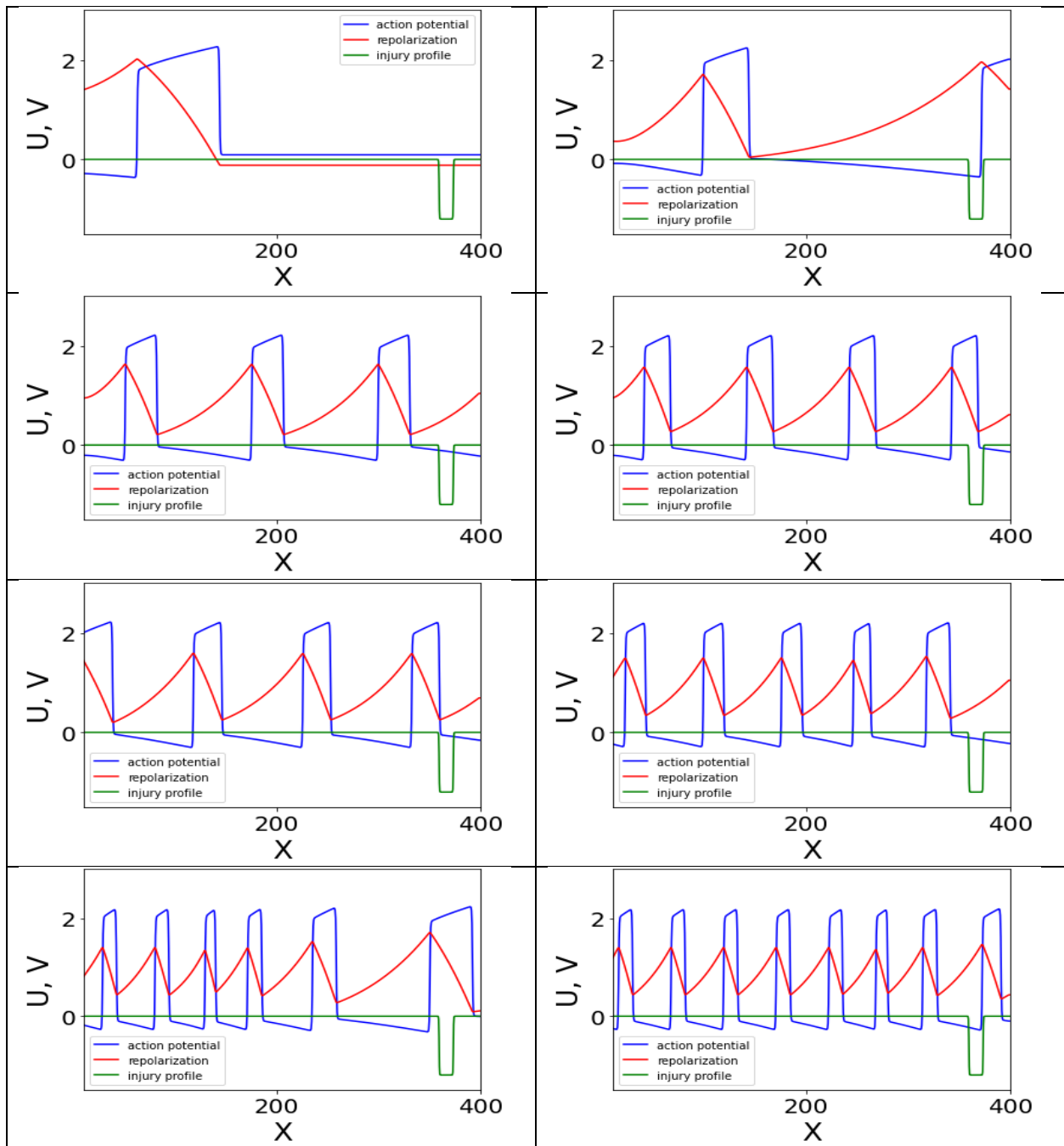
Figure 26 - Spatiotemporal evolution of action potential (blue curve) in PN with injury located at the end of cable shown in green. Red curve is a recovery variable. This evolution is determined at PN stimulations period equal to BCL$_{end}$ for $\alpha = 7.0$, $D_0 = 0.51$, $\delta = 0.45$. The length of the cable is set at the value of $400\Delta x$, time distance between snapshots is $26\Delta t$, time for the upper left snapshot is $6\Delta t$.

Figures 24-26 demonstrate that unlike the previous case (injury at the center of the cable) periodic stimuli applied at the left ends of the injured PNs initiate the propagation of AP waves with length and speed decreasing for greater values of D_0. Just like in the previous case, the AP waves gradually evolve in time until they reach developed steady state regimes. However, in this case, as D_0 increase the periods of time between successive APs get longer growing from $T_{F(24)} = 492\Delta t$ to $T_{F(25)} = 506\Delta t$ and $T_{F(26)} = 544\Delta t$ (Fig. 24 - 26).
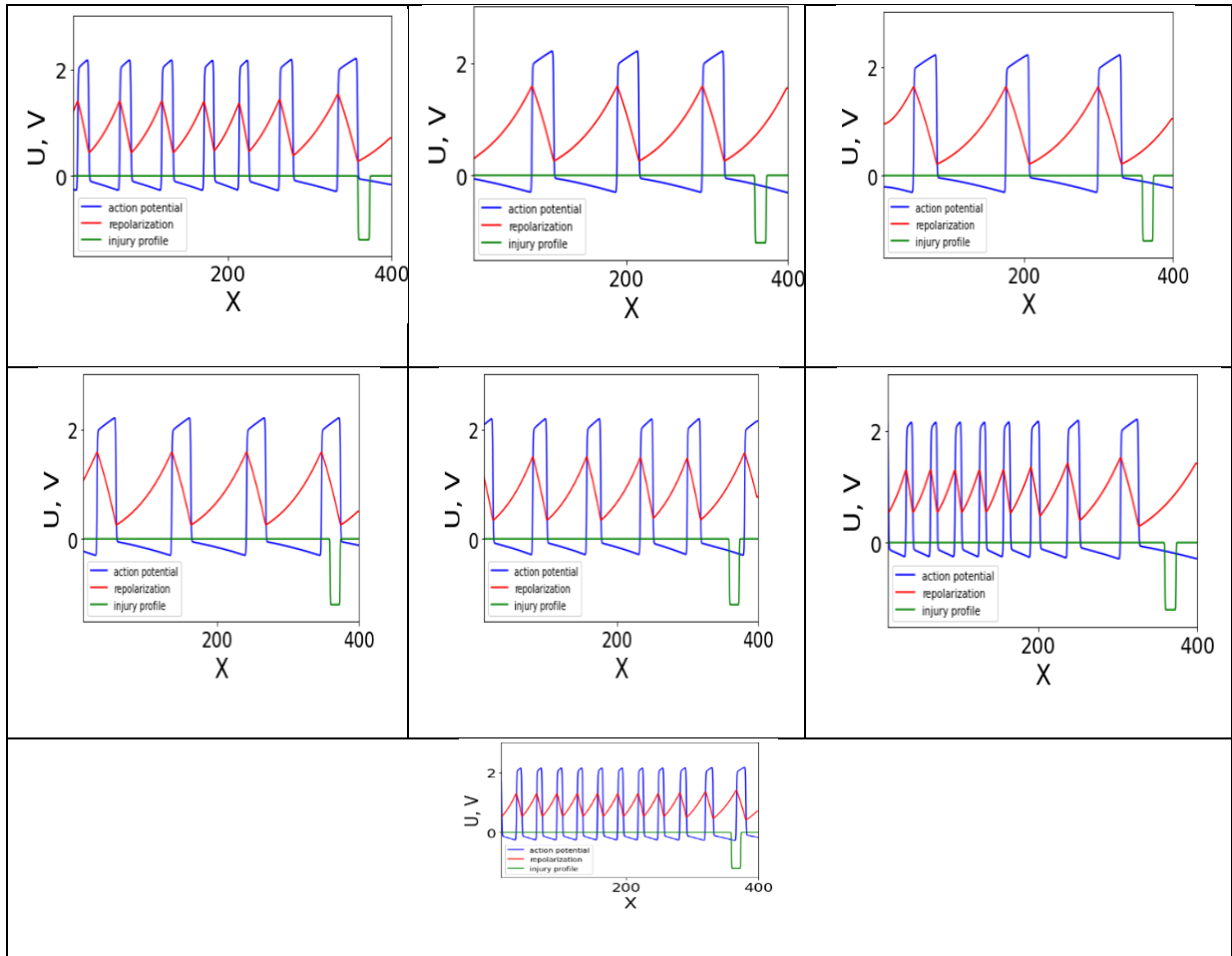
Figure 27 - Spatiotemporal evolution of action potential (blue curve) in PN with injury located at its center (first row) and end (second row). Similar sequence in PN without injury is shown in third row. Red curve is a recovery variable. Upper panels shown from left to right correspond to $D_0 = 0.49$, 0.5, and 0.51, respectively. Bottom panel relates to $D_0 = 0.51$. Stimulations applied at the left ends of PNs occur at periods equal to BCL$_{end}$. Other parameters are δ= 0.4. $\alpha = 7.0$.

Figure 27 readily demonstrates that as the value of D_0 increases the AP wavelength may get longer or shorter depending on location of the injury. Such alteration can be explained from the following considerations. If the injury is located at the center of PN, the AP wave does not have enough space to reach its steady state length and slows down sufficiently fast right after its initiation at the entrance of the nerve. It happens because the area of injury is somewhat too close to the entrance of PN. Such decelerated wave propagation contributes to the insertion of additional AP waves since the initial wave is sufficiently short. When injury is away from the entrance and closer to the end of the nerve, the initial AP wave accelerates significantly and gets substantially longer thus preventing the insertion of additional waves of comparable length. It should be noted that, as one would expect, regardless of values of D_0 the reported in Fig. 27 periods $T_{F(i)}$ are greater than the average BCL$_{end}$ estimate of $440\Delta t^1$ computed for the case of PN with no injury.

Discussion

It was observed that stability of AP propagation was different in injured and healthy nerves. We noticed that oscillations of BCL$_{end}$ were present in both healthy and injured PNs but

---

[1] Since simulations in injured PN were performed around $D_0 = 0.5$ we compared T_F measurements with similar D_0 values and mid values of nonlinear diffusion red curve in Fig. 13a, $d = 0.02, D_0 = 0.5$).

in injured PNs they had markedly higher amplitudes dependent on the nerve's length and the extension of its injured part. It has been noticed that at longer injuries the BCL_{end} oscillations did not significantly differ between longer and shorter PNs. However, at shorter injuries average BCL_{end} values were significantly shorter especially in the lower range of D_0 smaller than 0.5. Also, it was found that in healthy nerves BCL_{end} oscillations evolved with a positive diffusion dependent trend while the same oscillations in injured PNs occurred almost without a shift in equilibrium values of BCL_{end}. Furthermore, we noted a distinct alternating behavior in spatiotemporal evolution of AP waves in injured PNs with injuries at the center and at the end of the nerve.

Conclusion

We opine that it is reasonable to conclude that high amplitude oscillations of BCL_{end} analyzed in our model of excitation in injured PNs could be associated with tingling (short BCL_{end}) and numbness (prolonged BCL_{end}) typical for various peripheral neuro-pathologies associated with impaired electrical conductance[67]. Results of our study may improve monitoring of peripheral nerve growth and enhance adjustment of propagation of excitation to re-establish impaired connectivity in injured peripheral nerves.

CHAPTER IV: CONCLUSIONS

In this thesis, we investigated the stabilization of propagation in healthy and injured peripheral nerves with impaired electrical conductance. Current work on injured peripheral nerves, which is mostly limited to the medical field, focuses primarily on surgical interventions to repair severely damaged nerves without hopes of natural spontaneous recovery. In Chapter II and Chapter III, we were able to establish the theoretical framework that can help monitor the regrowth of injured peripheral nerves and also improve the propagation of excitation in such.

In Chapter I, we introduced models that can be used to describe excitability in excitable media in general. We also introduced some theoretical background that was used as a framework to develop the model we eventually used.

In Chapter II, we demonstrated that a 1D FN model which we modified to include nonlinear diffusion, is adequate to describe propagation of action potential in a small healthy peripheral nerve. We showed that every parameter of the nonlinear diffusion component plays a very important role in the stabilization of propagation in healthy peripheral nerves. We also observed that there was some form of dependency of stability on FN relaxation parameter ε. We further established the oscillatory dependance of BCL_{end} and APD_{end} on d in both the quadratic and quartic cases of the nonlinear diffusion. We found that while both BCL_{end} vs d and APD_{end} vs d curves trended positively upwards, the APD_{end} vs d curves generally presented lower amplitudes of oscillation in both quadratic and quartic cases.

In Chapter III, we modified the model from Chapter II even further by replacing its nonlinear diffusion coefficient d, with inhomogeneous diffusion $d^s(x)$ to model the area of injury in peripheral nerves. Due to severe demyelination in severe injury, we were considering,

there was a reduction in ionic conductance and complete conduction block. As a result of this conditions, we applied a stronger initial stimulus I_{stim}^{inj}, than when we investigated healthy peripheral nerves. To ensure that there was a stable propagation of excitation throughout the PN, we included additional stimuli which was 3% amplitude of the primary current initially applied at the left end of the cable. We went further to analyze the dependance of BCL_{end} and APD_{end} on D_0 for various lengths of the PN. We found that the dependance in both cases were oscillatory in behavior. Furthermore, we observed that irrespective of the spatial extension of the injury, the amplitude of BCL_{end} oscillation is higher in longer PNs than shorter ones. We concluded the chapter by showing the spatiotemporal evolution of action potential in PNs with injury at the center and at the end. We found that patterns of insertion of additional waves at the left end of the PN alternated depending on location of the injury.

REFERENCES

1. Grinsell, D. & Keating, C. P. Peripheral Nerve Reconstruction after Injury: A Review of Clinical and Experimental Therapies. *BioMed Res. Int.* **2014**, e698256 (2014).

2. Höke, A. A (heat) shock to the system promotes peripheral nerve regeneration. *J. Clin. Invest.* **121**, 4231–4234 (2011).

3. Irwin, M. & Wang, Z. Dynamic Systems Modeling. in *The International Encyclopedia of Communication Research Methods* (eds. Matthes, J., Davis, C. S. & Potter, R. F.) 1–12 (John Wiley & Sons, Inc., 2017). doi:10.1002/9781118901731.iecrm0074.

4. Brayton, R. & Tong, C. Stability of dynamical systems: A constructive approach. *IEEE Trans. Circuits Syst.* **26**, 224–234 (1979).

5. Issa, Z. F., Miller, J. M. & Zipes, D. P. 1 - Molecular Mechanisms of Cardiac Electrical Activity. in *Clinical Arrhythmology and Electrophysiology (Third Edition)* (eds. Issa, Z. F., Miller, J. M. & Zipes, D. P.) 1–14 (Elsevier, 2019). doi:10.1016/B978-0-323-52356-1.00001-3.

6. Miura, R. M. Analysis of excitable cell models. *J. Comput. Appl. Math.* **144**, 29–47 (2002).

7. Bak, P., Chen, K. & Tang, C. A forest-fire model and some thoughts on turbulence. *Phys. Lett. A* **147**, 297–300 (1990).

8. Keener, J. P. The Dynamics of Excitability. *Math. Biol.* 33.

9. Excitability. in *Mathematical Physiology* (eds. Keener, J. & Sneyd, J.) 116–159 (Springer, 1998). doi:10.1007/0-387-22706-7_4.

10. Herculano-Houzel, S. The human brain in numbers: a linearly scaled-up primate brain. *Front. Hum. Neurosci.* **3**, (2009).

11. Dharani, K. Chapter 2 - Physiology of the Neuron. in *The Biology of Thought* (ed. Dharani, K.) 31–52 (Academic Press, 2015). doi:10.1016/B978-0-12-800900-0.00002-6.

12. Davidovits, P. Chapter 13 - Electricity. in *Physics in Biology and Medicine (Fifth Edition)* (ed. Davidovits, P.) 193–211 (Academic Press, 2019). doi:10.1016/B978-0-12-813716-1.00013-6.

13. Menorca, R. M. G., Fussell, T. S. & Elfar, J. C. Peripheral Nerve Trauma: Mechanisms of Injury and Recovery. *Hand Clin.* **29**, 317–330 (2013).

14. Rigoard, P. *et al.* Organisation anatomique et physiologique du nerf périphérique. *Neurochirurgie* **55**, S3–S12 (2009).

15. Grinsell, D. & Keating, C. P. Peripheral Nerve Reconstruction after Injury: A Review of Clinical and Experimental Therapies. *BioMed Res. Int.* **2014**, 1–13 (2014).

16. Hammond, C. *Cellular and molecular neurophysiology*. (Elsevier/AP, Academic Press is an imprint of Elsevier, 2015).

17. Ramahi, A. A. & Ruff, R. L. Membrane Potential. in *Encyclopedia of the Neurological Sciences (Second Edition)* (eds. Aminoff, M. J. & Daroff, R. B.) 1034–1035 (Academic Press, 2014). doi:10.1016/B978-0-12-385157-4.00062-2.

18. Chrysafides, S. M., Bordes, S. & Sharma, S. Physiology, Resting Potential. in *StatPearls* (StatPearls Publishing, 2021).

19. Kogan, B. Y. *et al.* The simplified FitzHugh-Nagumo model with action potential duration restitution: Effects on 2D wave propagation. *Phys. Nonlinear Phenom.* **50**, 327–340 (1991).

20. Tse, G. *et al.* Cardiac dynamics: Alternans and arrhythmogenesis. *J. Arrhythmia* **32**, 411–417 (2016).

21. Hodgkin, A. L., Huxley, A. F. & Katz, B. Measurement of current-voltage relations in the membrane of the giant axon of *Loligo*. *J. Physiol.* **116**, 424–448 (1952).

22. Hodgkin, A. L. & Huxley, A. F. Currents carried by sodium and potassium ions through the membrane of the giant axon of *Loligo*. *J. Physiol.* **116**, 449–472 (1952).

23. Hodgkin, A. L. & Huxley, A. F. The components of membrane conductance in the giant axon of *Loligo*. *J. Physiol.* **116**, 473–496 (1952).

24. Hodgkin, A. L. & Huxley, A. F. The dual effect of membrane potential on sodium conductance in the giant axon of *Loligo*. *J. Physiol.* **116**, 497–506 (1952).

25. Hodgkin, A. L. & Huxley, A. F. A quantitative description of membrane current and its application to conduction and excitation in nerve. *J. Physiol.* **117**, 500–544 (1952).

26. Ermentrout, G. B. & Terman, D. H. *Mathematical Foundations of Neuroscience*. vol. 35 (Springer New York, 2010).

27. Meunier, C. & Segev, I. Playing the Devil's advocate: is the Hodgkin–Huxley model useful? *Trends Neurosci.* **25**, 558–563 (2002).

28. Fitzhugh, R. Thresholds and Plateaus in the Hodgkin-Huxley Nerve Equations. *J. Gen. Physiol.* **43**, 867–896 (1960).

29. FitzHugh, R. Impulses and Physiological States in Theoretical Models of Nerve Membrane. *Biophys. J.* **1**, 445–466 (1961).

30. Nagumo, J., Arimoto, S. & Yoshizawa, S. An Active Pulse Transmission Line Simulating Nerve Axon. *Proc. IRE* **50**, 2061–2070 (1962).

31. Zeldowitsch, J. B. & Frank-Kamenetzki, D. A. A Theory of Thermal Propagation of Flame. in *Dynamics of Curved Fronts* 131–140 (Elsevier, 1988). doi:10.1016/B978-0-08-092523-3.50015-0.

32. Dikansky, A. Fitzhugh-Nagumo equations in a nonhomogeneous medium. *Conf. Publ.* **2005**, 216 (2005).

33. Solving dynamic equations in dye transport. in *Modelling, Simulation and Control of the Dyeing Process* 100–113 (Elsevier, 2014). doi:10.1533/9780857097583.100.

34. Murray, J. D. *Mathematical biology*. (Springer, 2002).

35. Fisher, R. A. THE WAVE OF ADVANCE OF ADVANTAGEOUS GENES. *Ann. Eugen.* **7**, 355–369 (1937).

36. Newell, A. C. & Whitehead, J. A. Finite bandwidth, finite amplitude convection. *J. Fluid Mech.* **38**, 279–303 (1969).

37. Segel, L. A. Distant side-walls cause slow amplitude modulation of cellular convection. *J. Fluid Mech.* **38**, 203–224 (1969).

38. Plecko, B. & Steinfeld, R. 46 - Disorders of Vitamin Metabolism. in *Swaiman's Pediatric Neurology (Sixth Edition)* (eds. Swaiman, K. F. et al.) 373–382 (Elsevier, 2017). doi:10.1016/B978-0-323-37101-8.00046-1.

39. Plonsey, R. & Barr, R. C. *Bioelectricity: a quantitative approach*. (Springer, 2007).

40. Schmidt, H. & Knösche, T. R. Action potential propagation and synchronisation in myelinated axons. *PLOS Comput. Biol.* **15**, e1007004 (2019).

41. Wallisch, P. Fitzhugh-Nagumo Model. in *MATLAB for Neuroscientists* 425–438 (Elsevier, 2014). doi:10.1016/B978-0-12-383836-0.00030-8.

42. Anderson, B. C. & McLoon, L. K. Cranial Nerves and Autonomic Innervation in the Orbit. in *Encyclopedia of the Eye* (ed. Dartt, D. A.) 537–548 (Academic Press, 2010). doi:10.1016/B978-0-12-374203-2.00285-2.

43. Baker, R. & Precht, W. Electrophysiological properties of trochlear motoneurons as revealed by IVth nerve stimulation. *Exp. Brain Res.* **14**, (1972).

44. Mayer, A., Bittihn, P. & Luther, S. Complex restitution behavior and reentry in a cardiac tissue model for neonatal mice. *Physiol. Rep.* **5**, e13449 (2017).

45. Starobin, J. M. & Varadarajan, V. Entrainment of marginally stable excitation waves by spatially extended sub-threshold periodic forcing. *Nonlinear Biomed. Phys.* **5**, 8 (2011).

46. Lundborg, G., Dahlin, L. B., Danielsen, N. & Nachemson, A. K. Tissue specificity in nerve regeneration. *Scand. J. Plast. Reconstr. Surg.* **20**, 279–283 (1986).

47. Huang, Y.-C. & Huang, Y.-Y. Biomaterials and strategies for nerve regeneration. *Artif. Organs* **30**, 514–522 (2006).

48. Danielsen, N., Dahlin, L. B., Ericson, L. E., Crenshaw, A. & Lundborg, G. Experimental hyperthyroidism stimulates axonal growth in mesothelial chambers. *Exp. Neurol.* **94**, 54–65 (1986).

49. Ciardelli, G. & Chiono, V. Materials for peripheral nerve regeneration. *Macromol. Biosci.* **6**, 13–26 (2006).

50. Grinsell, D. & Keating, C. P. Peripheral Nerve Reconstruction after Injury: A Review of Clinical and Experimental Therapies. *BioMed Res. Int.* **2014**, e698256 (2014).

51. Flores, A. J., Lavernia, C. & Owens, P. Anatomy and physiology of peripheral nerve injury and repair. *Am. J. Orthop. Belle Mead NJ* **29**, 167–73 (2000).

52. Ducker, T. B., Kempe, L. G. & Hayes, G. J. The metabolic background for peripheral nerve surgery. *J. Neurosurg.* **30**, 270–280 (1969).

53. Lieberman, A. R. The axon reaction: a review of the principal features of perikaryal responses to axon injury. *Int. Rev. Neurobiol.* **14**, 49–124 (1971).

54. Son, Y. J. & Thompson, W. J. Schwann cell processes guide regeneration of peripheral axons. *Neuron* **14**, 125–132 (1995).

55. Seddon, H. J. A Classification of Nerve Injuries. *Br Med J* **2**, 237–239 (1942).

56. Burnett, M. G. & Zager, E. L. Pathophysiology of peripheral nerve injury: a brief review. *Neurosurg. Focus* **16**, 1–7 (2004).

57. SUNDERLAND, S. A CLASSIFICATION OF PERIPHERAL NERVE INJURIES PRODUCING LOSS OF FUNCTION. *Brain* **74**, 491–516 (1951).

58. Thomas, P. K. & Holdorff, B. Neuropathy due to physical injury. (1993).

59. Ramachandran, S. & Midha, R. Recent advances in nerve repair. *Neurol. India* **67**, S106–S114 (2019).

60. Wolford, L. M. & Stevao, E. L. L. Considerations in nerve repair. *Proc. Bayl. Univ. Med. Cent.* **16**, 152–156 (2003).

61. P, M., S, H., M, D. & M, S. Advances of Peripheral Nerve Repair Techniques to Improve Hand Function: A Systematic Review of Literature. *Open Orthop. J.* **6**, 60–68 (2012).

62. Bhandari, P. S. Management of peripheral nerve injury. *J. Clin. Orthop. Trauma* **10**, 862–866 (2019).

63. Yildiz, N. NERVE IMPLANTS. in *Medical Textiles and Biomaterials for Healthcare* (eds. Anand, S. C., Kennedy, J. F., Miraftab, M. & Rajendran, S.) 441–447 (Woodhead Publishing, 2006). doi:10.1533/9781845694104.7.441.

64. Kornfeld, T., Vogt, P. M. & Radtke, C. Nerve grafting for peripheral nerve injuries with extended defect sizes. *Wien. Med. Wochenschr. 1946* **169**, 240–251 (2019).

65. Narakas, A. O. & Hentz, V. R. Neurotization in brachial plexus injuries. Indication and results. *Clin. Orthop.* 43–56 (1988).

66. Rasulić, L. *et al.* Useful functional recovery and quality of life after surgical treatment of peroneal nerve injuries. *Front. Surg.* **9**, 1005483 (2022).

67. Hochman, J. R., French, M. R., Bermingham, S. L. & Hawker, G. A. The nerve of osteoarthritis pain. *Arthritis Care Res.* **62**, 1019–1023 (2010).

APPENDIX A: COMPUTATION FOR COMPARISON OF RESTITUTION

```python
"""Created by Olu Oni at 10/21/20
"""
Program to compute comparison between linear and nonlinear restitution
"""
import numpy as np
from matplotlib import pyplot as plt

# Geometry
x1 = 0
x2 = 400

# Spatial grid
dx = .5
nx = int((x2 - x1) / dx)
x = np.linspace(x1, x2, nx)

# Time grid
dt = dx / 10
nt = 100000

# media property

epsilon = 0.005
gamma = 2.0
a = -2.0
u0, u1, u2 = 0, .63, 2.25
diff = u2 - u1
check = 0
check1 = True
counter = 0
amax = 9.0
q = 5.0
flag = False
kmax = 120
kcount = 0
taStart = 0
taEnd = 0
startTimer = 0
endTimer = 0


def f(x, u0, u1, u2):
    """
```

```python
        reaction function for FitzHugh Nagumo model
        :param x: independent variable
        :param u0: typically 0
        :param u1: point of equilibrium 1
        :param u2: point of equilibrium 2
        :return: the function a(x-u0)(x-u1)(x-u1)
        """
        return a * (x - u0) * (x - u1) * (x - u2)


    def diff_func(d):
        return d

    def diff_func_D(D0, d, u):
        """non-linear diffusion function"""
        return D0 + d * u ** 2


    def fn_computation(kcount, flag, startTimer, endTimer, taStart, taEnd, epsilon, gamma,
D0, d, dk, testSpot,
                   status):
        global label
        u = np.zeros(nx)
        v = u
        APD_plot = []
        DI_plot = []
        print(coeffs)
        time = np.zeros((kmax, 2))

        for k in range(kmax):
            period = 12007 - k * dk
            tapd = []
            tdi = []

            for n in range(1, nt + 1):
                # continuous propagation
                if n % period == 0:
                    u[0:10] = u2 - u1

                un = u.copy()
                vn = v.copy()
                if status == "nlinear":
                    u[1:-1] = un[1:-1] + dt * (f(un[1:-1], u0, u1, u2) - vn[1:-1]) + diff_func_D(D0,
d, un[1:-1]) * \
                            (dt / dx ** 2) * (un[2:] - 2 * un[1:-1] + un[0:-2])
                    label = f"{D0} + ${d}*u^2$"
```

```python
        else:
            u[1:-1] = un[1:-1] + dt * (f(un[1:-1], u0, u1, u2) - vn[1:-1]) + diff_func(D0) * \
                    (dt / dx ** 2) * (un[2:] - 2 * un[1:-1] + un[0:-2])
            label = f"$D_0 = {D0}$"
            # setting Boundary Conditions
        u[0] = u[2]
        u[-1] = u[-3]
        v = vn + dt * (epsilon * (gamma * un - vn))

        if not flag and u[testSpot] > 0.5:
            flag = True

        if abs(u[testSpot] - v[testSpot]) < 0.01 and u[testSpot + 10] < u[testSpot] and
startTimer < 0 and flag:
            taStart = n
            tdi.append(taStart - taEnd)
            startTimer = 500

        if abs(v[testSpot] - u[testSpot]) < 0.01 and u[testSpot + 10] > u[testSpot] and
endTimer < 0 and flag:
            taEnd = n
            tapd.append(taEnd - taStart)
            # count += 1
            endTimer = 500

        startTimer -= 1
        endTimer -= 1
    if tapd:
        if (tapd[-1] - tapd[-2]) < 10 and (tdi[-1] - tdi[-2]) < 10:
            try:

                time[kcount, :] = [tapd[-1] * dt, tdi[-1] * dt]
                print([tapd[-1] * dt, tdi[-1] * dt])
            except IndexError:
                addition = np.array([tapd[-1] * dt, tdi[-1] * dt])
                time = np.vstack((time, addition))
        else:
            break
    kcount += 1
time = time[~np.all(time == 0, axis=1)]
plt.scatter(time[:, 1], time[:, 0], label=label, )
plt.plot(time[:, 1], time[:, 0])
plt.xticks(fontsize=15)
plt.yticks(fontsize=15)
return [tapd[-1] * dt, tdi[-1] * dt]
```

```python
        D = [1.0, ]
        coeffs = [ .02,.03, .04, .05]
        for D0 in D:
            for d in coeffs:
                fn_computation(kcount, flag, startTimer, endTimer, taStart, taEnd, epsilon, gamma,
D0, d, dk=160, testSpot=100,
                        status="nlinear")
                print("\n")
                fn_computation(kcount, flag, startTimer, endTimer, taStart, taEnd, epsilon, gamma,
D0, d, dk=160,
                        testSpot=100, status="linear")

            plt.ylabel(r'APD ,$\Delta t$', fontsize=20)
            plt.xlabel(r'RI ,$\Delta t$', fontsize=20)
            plt.xticks([250, 350, 450], fontsize=25)
            plt.yticks([80, 90, 100, 110, 120,], fontsize=25)
        plt.show()
    plt.show()
```

```python
from matplotlib import pyplot as plt
import pandas as pd
import numpy as np
"""
Created on Wed Nov 25 08:45:08 2021

@author: OTONI
"""

"""
# Created by Olu Oni at 10/21/20

"""

Program to compute the end of APD and BCL
"""

# Geometry
x1 = 0
x2 = 400

# Spatial grid
dx = .5
nx = int((x2 - x1) / dx)
xx = np.linspace(x1, x2, nx)

# Time grid
dt = dx / 10
nt = 100000

# media property

epsilon = 0.005
gamma = 2.0  # 2.0 original
a = -2.0
u0, u1, u2 = 0, .63, 2.25
diff = u2 - u1
check = 0
check1 = True
counter = 0
amax = 9.0
q = 5.0
flag = False
kmax = 120
```

```python
kcount = 0
taStart = 0
taEnd = 0
startTimer = 0
endTimer = 0
checker = True
checker1 = True
I_stim = 0.0045


def heaviside_funct():
    t = np.linspace(0, 10, 398)
    N = len(t)
    A = 0.005
    shift = 0
    u = np.zeros(N)
    for i in range(0, N):
        if t[i] >= -shift:
            u[i] = A
    return u


def f(x, u0, u1, u2):
    """
    reaction function for FitzHugh Nagumo model
    :param x: independent variable
    :param u0: typically 0
    :param u1: point of equilibrium 1
    :param u2: point of equilibrium 2
    :return: the function a(x-u0)(x-u1)(x-u1)
    """
    return a * (x - u0) * (x - u1) * (x - u2)


def diff_func(d):
    return d


def diff_func_D(D0, d, u):
    """non-linear diffusion function"""
    return D0 + d * u ** 2


def new_diff_func_D(D0, u, x, sigma, a, c):
    return D0 + sigma * (np.tanh(3 * (x + a)-c) - np.tanh(3 * (x - a)-c)) * u ** 2
```

```python
def fn_computation(kcount, flag, startTimer, endTimer, taStart, taEnd, epsilon, gamma,
D0, dk, testSpot):
    global label, checker, n
    df = pd.DataFrame(columns=['x', 'APD', 'DI', 'BCL',])
    u = np.zeros(nx)
    v = u
    xvalue = [0]

    # injury profile
    x1 = np.linspace(0, 400, 1000)
    s = -0.5
    b = 3.0
    a = 7.0
    d = 0.12 * 10
    c = 600
    y1 = s*d*(np.tanh(b*(x1+a)-c) - np.tanh(b*(x1-a)-c))

    for x in xvalue:
        time = np.zeros((kmax, 2))
        for k in range(kmax):
            period = (12007 - k * dk)
            tapd = []
            tdi = []
            if period < 0:
                break

            for n in range(1, nt + 1):
                # continuous propagation
                if n % (period) == 0:
                    u[0:10] = (u2 - u1)/2.5
                un = u.copy()
                vn = v.copy()
                u[1:-1] = I_stim + un[1:-1] + dt * (f(un[1:-1], u0, u1, u2) - vn[1:-1]) +
new_diff_func_D(D0, u[1:-1], x, sigma=0.1, a=2.0,c=1050) * \
                        (dt / dx ** 2) * (un[2:] - 2 * un[1:-1] + un[0:-2])
                label = f"{D0} + ${0.5 * (np.tanh(3 * (x + 2.0)) - np.tanh(3 * (x - 2.0)))}*u^2$
for x = {round(x, 3)}"


                # setting Boundary Conditions
                u[0] = u[2]
                u[-1] = u[-3]
                v = vn + dt * (epsilon * (gamma * un - vn - 0.4))
                if not flag and u[testSpot] > 0.5:
                    flag = True
```

```
                    if abs(u[testSpot] - v[testSpot]) < 0.01 and u[testSpot + 10] < u[testSpot] and
startTimer < 0 and flag:
                        taStart = n
                        tdi.append(taStart - taEnd)
                        startTimer = 500

                    if abs(v[testSpot] - u[testSpot]) < 0.01 and u[testSpot + 10] > u[testSpot] and
endTimer < 0 and flag:
                        taEnd = n
                        tapd.append(taEnd - taStart)
                        # count += 1
                        endTimer = 500

                    startTimer -= 1
                    endTimer -= 1



                if len(tapd) > 1:
                    if (tapd[-1] - tapd[-2]) < 10 and (tdi[-1] - tdi[-2]) < 10:
                        try:
                            time[kcount, :] = [tdi[-1] * dt, tapd[-1] * dt]
                            data1 = pd.DataFrame(u)
                        except IndexError:
                            addition = np.array([tdi[-1] * dt, tapd[-1] * dt])

                            time = np.vstack((time, addition))
                    kcount += 1
                xmax, ymax = time.max(axis=0)

                time = time[~np.all(time == 0, axis=1)]
                if x == 0:
                    plt.scatter(time[:, 0] + time[:, 1], time[:, 0],)
                data = pd.DataFrame(time)
                # data.to_excel(f'sample_data{D0}_1.xlsx', sheet_name=f'{D0}', index=True)

                try:
                    df = df.append({'x': x, 'DI': time[-1][0], 'APD': time[-1][1], 'BCL':time[-1][0] +
time[-1][1]}, ignore_index=True)
                except IndexError:
                    # break
                    pass
            return df

        def collated_calc(D, coeffs):
            df1 = pd.DataFrame({'x': coeffs})
```

```python
        ax = None
        for D0 in D:
            print(D0)

            df = fn_computation(kcount, flag, startTimer, endTimer, taStart, taEnd,
                        epsilon, gamma, D0, dk=160, testSpot=200,
                        )
            print("\n")
            print(df)
            leg = plt.legend(loc='upper left', ncol=2, mode=None, shadow=True,
fancybox=True)
            leg.get_frame().set_alpha(0.5)
            plt.title("Plot of restitution for various corresponding to alpha = 4.0 with Istim")
            plt.xlabel("BCL")
            plt.ylabel("APD")
            plt.show()
            df1 = df
            df1.columns = ['i', 'DI', f'APD for D0 = {D0}', f'BCL for D0 = {D0}']
        return df1
    D = [.52,]
    xvalue = [0.0]
    soln = collated_calc(D, xvalue)
```